Quaternary Science Advances 15 (2024) 100229

Contents lists available at ScienceDirect

Quaternary Science Advances

journal homepage: www.sciencedirect.com/journal/quaternary-science-advances

Quaternary environment and climate change reconstruction from geochemical and geoarchaeological evidences of paleosols in east-central Barind, NW Bangladesh

Md. Sha Alam [a], Md. Shafiqul Alam [b], Mohammad Nazim Zaman [c], Ayon Saha [d], Md Mahmudul Hasan Rakib [d], Arabe Khan [d], Rahat Khan [e], Dhiman Kumer Roy [d,*]

[a] Institute of Mining, Mineralogy and Metallurgy (IMMM), Bangladesh Council of Scientific and Industrial Research (BCSIR), Joypurhat, Bangladesh
[b] Department of Geology and Mining, University of Rajshahi, Bangladesh
[c] Bangladesh Council of Scientific and Industrial Research (BCSIR), Dhaka, Bangladesh
[d] Department of Geology and Mining, University of Barishal, Barishal, Bangladesh
[e] Institute of Nuclear Science & Technology, Bangladesh Atomic Energy Commission (BAEC), Savar, Dhaka, 1349, Bangladesh

ARTICLE INFO

Keywords:
Quaternary deposit
Paleosol
Geoarchaeology
Weathering index
Paleoclimate

ABSTRACT

This research focuses on analyzing paleosols, major and trace element geochemistry, organic carbon levels, and geo-archaeological aspects of Quaternary deposits investigated in two sedimentary successions located in the east-central Barind region of NW Bangladesh. Several factors that influence the paleosol development can be used to decipher the paleoenvironment and paleoclimatic conditions of the study area. Sedimentary succession of the studied sections have been grouped into two broad categories i.e., Gray unit/Newer Alluvium (NA) of Late Holocene and Red unit/Older Alluvium (OA) of Early Pleistocene age. Some geoarchaeological evidences have been found at the bottom of the gray unit and the top of the red unit in Durgadaha (DD) section indicating the existence of paleo-settlement at about ~1300 years BP. The age is determined by the relative dating of several artifacts found at the paleo-settlement surface. Interpretation of several field characteristics and geochemical parameters i.e., clayeyness, salinization, base loss, calcification, leaching (Ba/Sr), aeolian input (Zr/Al), CIA, CIW, CIA-K, etc. revealed that the paleosols in gray unit are weakly developed; whereas, paleosols in red unit are relatively moderate, strong to very strongly developed. In the red unit, the MAP and MAT range from 1000 ± 181 mm to 1478 ± 181 mm and 9° ± 4.4°–14° ± 4.4 °C respectively. On the other hand, MAT ranges from 23.1° ± 0.6 °C to 28.3° ± 0.6 °C in gray unit paleosols. Depending on the depositional pattern and estimated MAT, five short-term climatic cycles (i.e., alternating phases of dry and wet) have been recognized in gray/newer alluvium units during the last 1300 years. The demise of paleo settlement (1300 years BP) due to the abrupt climatic change towards a dry and cooler phase where the MAT was estimated as 23.1° ± 0.6° which is at least 3 °C lower than the present. This study also revealed that the estimated MAP and MAT are more analogous to paleoclimatic records of the Asian regions.

1. Introduction

Quaternary continental paleoenvironmental and paleoclimatic conditions have been reconstructed by recognition and use of paleosols and it is now widely used for paleoclimatic research (Birkeland, 1984; Caran, 1998; Sheldon and Tabor, 2009; Tabor and Myers, 2015; Beverly et al., 2018; da Silva Neto et al., 2020; Raigemborn et al., 2023). Paleosols are soils that formed on the landscape in the past, which have direct interaction with climatic and environmental conditions that prevailed at the time of their development (Birkeland, 1984; Kraus, 1999; Retallack, 2008; Muhs, 2021). Climate, organism, topography, parent material, and time control the soil-forming processes (Birkeland, 1984; Huot et al., 2015; Matchavariani, 2019; Ben Mahmoud and Zurqani, 2021; Certini and Scalenghe, 2023). Precipitation and temperature are the vital factors that govern the degree of pedogenesis (i.e., soil development) and weathering processes along with the elemental mobility in paleosol (Kumaravel et al., 2009; Babeesh et al., 2017; Kogler and Hembree, 2019; Ghasera and Rashid, 2024). Leaching, transfer, and

* Corresponding author.
E-mail address: ddkroy@bu.ac.bd (D.K. Roy).

https://doi.org/10.1016/j.qsa.2024.100229
Received 3 May 2024; Received in revised form 6 August 2024; Accepted 7 August 2024
Available online 10 August 2024

dissolution of the major and trace elements during pedogenesis are also controlled by the chemical composition of the parent rock and the surface/groundwater flow (Nesbitt and Young, 1982, 1984, 1989; Maynard, 1992; McLennan et al., 1993; Li et al., 2014; Mikkonen et al., 2018; Moussavi-Harami et al., 2009; Naiman et al., 2005; Nash, 2022). Several studies show deviations of geochemical behavior through a paleosol profile provide evidence of the degree of pedogenesis and climatic conditions that existed during paleosol development (Wright, 1992; Retallack, 1995; Sheldon et al., 2002; Sheldon, 2003; Hou et al., 2022; Wang et al., 2023).

Several geochemical proxies have been widely used in paleosols to calculate chemical weathering with pedogenesis to infer paleoenvironment and paleoclimate (Delgado et al., 2021; Raigemborn et al., 2022; Srivastava et al., 2019; Tabor and Myers, 2015; Wang et al., 2023). The most important major element geochemical indices such as Clayeyness, Salinization, Base loss, and Calcification were proposed by Nesbitt and Young (1984) and also widely used in the literature (Prochnow et al., 2006; Sheldon, 2006; Beverly et al., 2018; Eze et al., 2021; Guo et al., 2024; Matshameko et al., 2022). Major element geochemical indices are CIA (Nesbitt and Young, 1982), CIW (Harnois, 1988), and CIA-K (after (Nesbitt and Young, 1982; Maynard, 1992) are used to calculate the overall condition of weathering processes. Estimation of carbon isotope values and concentration of Total Organic Crabon (TOC) in the sediments and paleosol are important to understand paleovegetation and past climatic conditions (Chen et al., 2011; Hussain et al., 2019; Yang et al., 2021; Varela et al., 2021). Total organic carbon (TOC) is a fundamental parameter for describing the abundance of organic content in soil or sediments (Meyers and Lallier-Vergès, 1999). Recently, several geochemical climofunctions for paleosols i.e., Mean Annual Precipitation (MAP) in mm and Mean Annual Temperature (MAT) in °C have been successfully applied in several continental parts of the world to reconstruct paleoenvironment and paleoclimate (Maynard, 1992; Sheldon et al., 2002; Sheldon and Retallack, 2004; Schatz et al., 2015; Gong et al., 2023; Aquino et al., 2024). Field recognition of paleosols and their geochemical characteristics is the most powerful tool for reconstructing paleoenvironment and climate when it is applied together with their depositional facies and geomorphic studies (Sheldon and Tabor, 2009; Retallack, 2016; N J Tabor et al., 2017). In addition, geoarchaeological findings buried in fluvial sequences can be excellent tools for paleoenvironmental interpretation (Ripley, 1998; Carey et al., 2017; Goiran et al., 2022). The Paleo-settlement history of a region is closely related to the availability of water, transportation, flora, fauna, andsuitable terrain for agriculture and river dynamics. All of these suitable conditions for establishing a settlement on a paleo-landscape are also closely connected to favorable climatic conditions.

The present study has been carried out on two sedimentary successions in an area of East-central Barind Tract, Joypurhat District, NW Bangladesh. The Barind tract is one of the most important Quaternary geomorphic units of the Bengal Basin. The study area experienced numerous erosional (deeply incised valley) and depositional processes (alluvial, floodplain, terrace, natural levee, bars) during the Late Holocene time and therefore Recent floodplain developed over the Barind clay residuum (Khan, 1991; Mukherjee et al., 2009; Neidhardt et al., 2013; Alam and Khan, 2022). Both the remnant of Barind deposits and the recent floodplain comprise a number of paleosols and numerous geoarchaeological evidence (Monsur and Paepe, 1992; Alam et al., 2008; Kumar et al., 2020). Quaternary paleosols in Barind Tract have been studied earlier from various perceptions based on field characterization (Alam, 1993; Monsur, 1995; Rashid and Islam, 2018), stable Carbon and Oxygen isotopic signatures of soil $CaCO_3$ (Alam, 1993; Alam et al., 1997) and rock magnetic-paleoclimatic signatures (Alam, 1993; Monsur and Paepe, 1992; Alam and Paepe, 1996, Alam et al., 1997). However, very little is known about the major element geochemical relations of the paleosols in the study area in terms of various weathering indices and climofunctions. Therefore, field observation and geochemical compositions have been used to decipher the paleoenvironment and paleoclimate of Pleistocene-Holocene paleosol. Geoarchaeological evidences found in the sedimentary sequences have also been studied to understand the growth and dynamics of paleosettlements linked to different climatic episodes.

2. Geological settings

The study area lies within the east-central Barind Tract, Joypurhat District, NW Bangladesh (Fig. 1). The Barind Tract is one of the major physiographic units of the Bengal Basin and represented as tectonically uplifted Pleistocene outcrop (Morgan and McIntire, 1959; Khandoker, 1987; Khan and Rahman, 1992; Monsur and Paepe, 1992; Alam et al., 1997; Kuehl et al., 2005; Rudra, 2018; Grimaud et al., 2020). The east-central portion of the Barind Tract is floodplain area and the deposits is directly overlie the tectonic element called Gaibanda-Nawabgonj Intracratonic High, which is a linear feature trending NE-SW (Khandoker, 1987; Khan and Rahman, 1992; Alam et al., 1997; Rashid et al., 2015). This linear feature has remained as a positive landmass since the Gondowana period and is bounded by a major basement fault. Reactivations of these basement faults have taken place from time to time, especially since the deposition of Early Pleistocene sediments of the Barind Tract (Khandoker, 1987). The sedimentary sequences of the Quaternary deposits of the area consist of Pleistocene brown, yellowish red to reddish yellow clay, silty clay to fine sand which is overlain by mostly gray color clayey silt and sands of Holocene age (Achyuthan and Thirunavukarasu, 2009; Nandy and Nath, 2021). The Holocene sediments were deposited by the Tista River and its distributary channel. The Quaternary deposits of the area contain several paleosol horizons. Bangladesh Meteorological Department (BMD) measured the study area receives a mean annual precipitation of 1700 mm and a mean annual temperature of about 26 °C.

3. Methodology

3.1. Field recognition of paleosols and sampling

Two excavated stratigraphic sections (Fig. 2) in the Joypurhat area of East-central Barind Tract, NW Bangladesh were selected for field recognition of paleosols and sample collection. These two sections DD and KS named after Durgadaha and Kujishahar localities lie within 25°4′ 40″ N and 25°5′00″ N latitude and 88° 55′ 9″and 88°59′5″ E longitude respectively. The elevation (AMSL) and the total thickness of the DD section are 25 m and 5.3 m respectively. On the other hand, a 6 m thick KS section is situated at an elevation of 23 m (AMSL). Field description of paleosols includes different pedogenic and biogenic features such as root traces, animal burrows, soil structures, slickensides, harmonization, color, mottling, Fe-Mn concretion, etc. were studied carefully followed after Birkeland (1984). Munsell Color Chart (Munsell, 1975) was used to determine the different colors of the sediments. Paleosols were classified based on field observations and US taxonomic system (Soil Survey Staff, 1999; Baillie, 2001). A total of 32 samples were collected from different recognized paleosols horizons of DD (n = 20) and KS (n = 12) sections and sealed into labeled plastic bags.

3.2. Laboratory procedure

A total 32 selected samples from different paleosol horizons and sedimentary units (Fig. 2) have been selected for XRF analysis. Each sample were crushed for 20 min in a Planetary Ball Mill (PM-200, Retsch, Germany) to make powder form in well-mixing conditions. Powdered samples were then pulverized in a pulverizer machine. Then finely ground powder (<100 μm) were put in a porcelain crucible and dried at 100 °C in an oven for 24 h to remove moisture. Dried powder samples were mixed with binder (steric acid with sample at a ratio of 1:10) and pulverized for 2 min. The mixture was spooned into an aluminum cap (30 mm) and sandwiched between two tungsten carbide

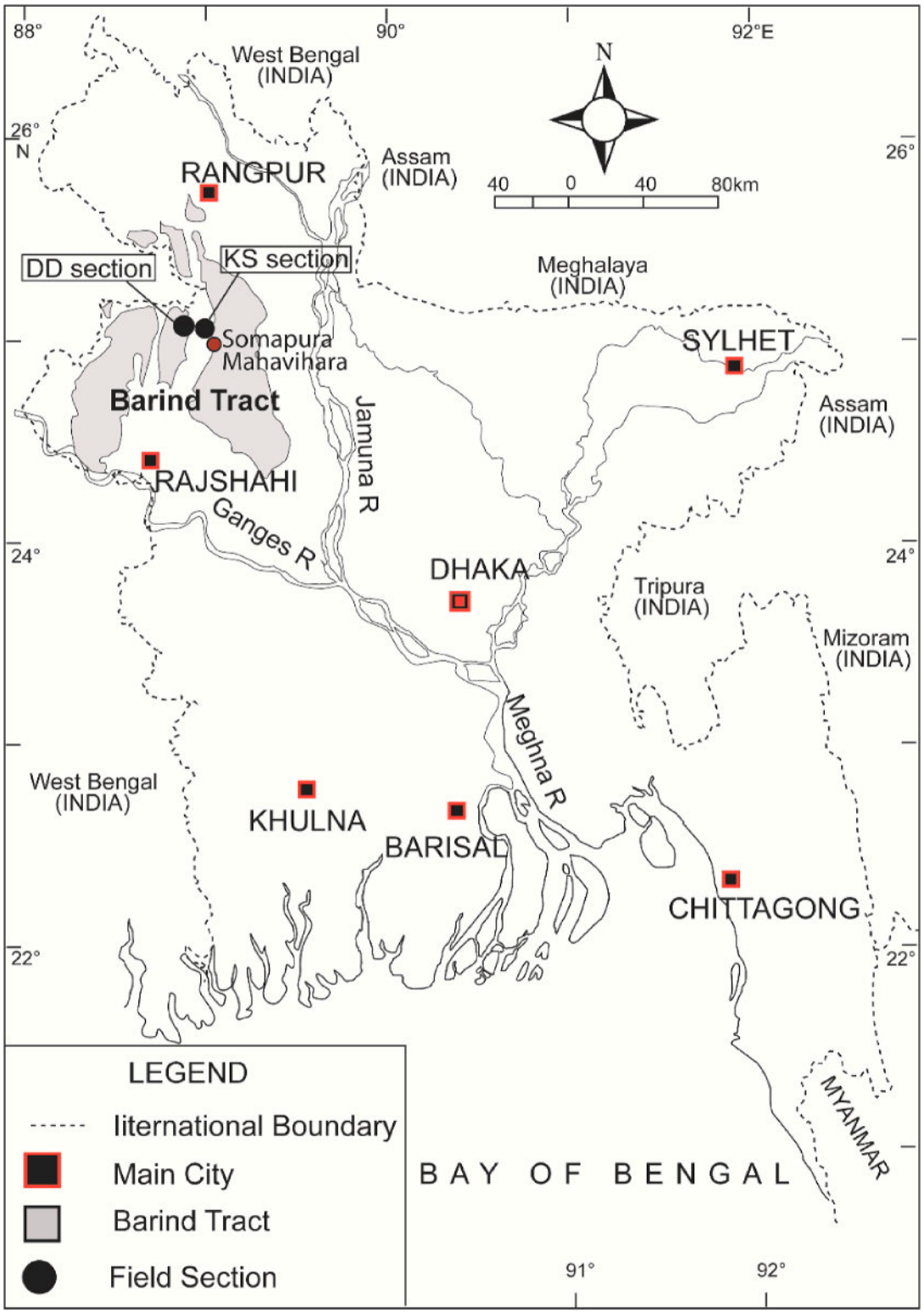

Fig. 1. Location map and position of field sections of the study area.

pellets using a manual hydraulic press with 10–15 tons/sq. in. for 2 min. Then the pressure released slowly and the pellets were t ready for X-ray Fluorescence (XRF) analysis. Major oxides and trace elements were determined at IMMM, BCSIR, Joypurhat by X-ray Fluorescence (XRF) Spectrometer method following the standard procedure as described by Rigaku Corporation using Rigaku ZSX Primus XRF machine equipped with an end window 4. kW Rh-anode X-ray tube. Analytical uncertainties for XRF major elements are <2% and trace elements are <10% (Rousseau, 2001; Saha et al., 2023) The loss on ignitions (LoI) were determined by igniting the samples at 950 °C temperature.

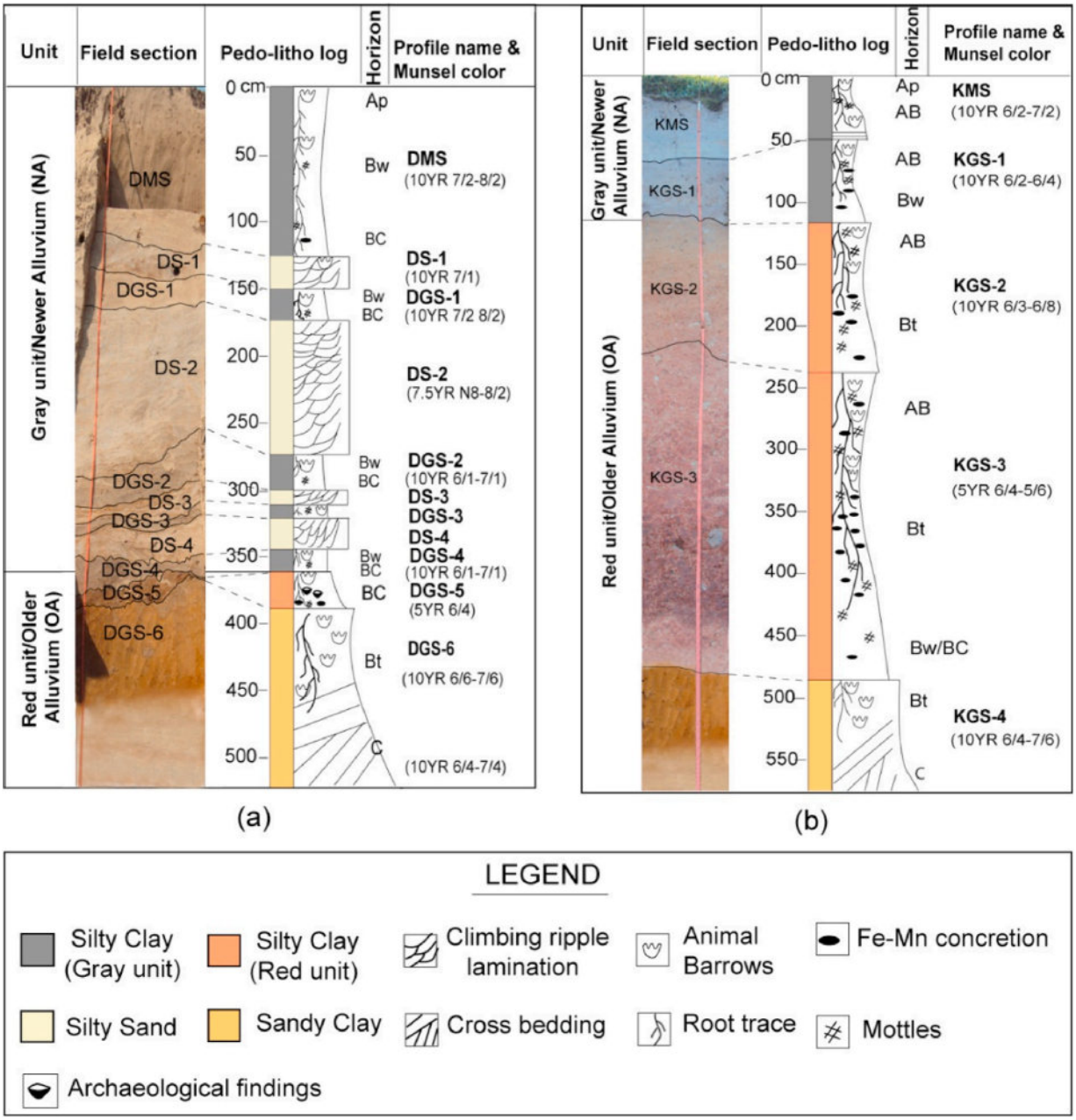

Fig. 2. Field classification of different soil/paleosols and sediment units in two sedimentary succession, i.e., (a) Durgadaha (DD) section where paleosols (i.e., DMS, DGS-1 to DGS-4, DGS-5, and DGS-6) are alternated with the silty sand horizon (i.e., DS-1 to DS-4), and (b) Kujishahar (KS) Section, where paleosol are classified as KMS, KGS-1, KGS-2, KGS-3 and KGS-4. Among the paleosols, DGS-5, DGS-6, KGS-2, KGS-3 and KGS-4 are belong to the red unit/older alluvium (OA) unit whereas the rest are within the gray unit/newer alluvium (NA) unit.

3.3. Analytical procedure

3.3.1. Chemical proxies

Several geochemical indices have been calculated by the molecular proportion of major and trace elements to infer geochemical characteristics during the weathering and pedogenesis of paleosols. The indices Clayeyness (Al_2O_3/SiO_2), Salinization ($Na_2O + K_2O)/Al_2O_3$), Base loss ($Al_2O_3/Na_2O + K_2O + CaO + MgO$), Calcification ($CaO + MgO/Al_2O_3$) have been calculated after Nesbitt and Young (1982 1984) and Sawyer (1986) to understand the relative strength of weathering and pedogenic conditions of the studied soil paleosol sequences. The molecular ratios of Ti/Al were calculated to determine source rock composition (Kurtz et al., 2000; Li, 2000; Stiles and Stensvold, 2008; Sheldon and Tabor, 2009; Chen et al., 2013; Rubinić et al., 2014; Liivamägi et al., 2021).

The trace element ratio of Ba/Sr and Sr/Rb were calculated to understand leaching and evaporation conditions during weathering and soil forming processes (Sheldon, 2006a; Retallack, 2001b; Roy et al., 2009; Amorosi et al., 2021; Profe et al., 2018). the Zr/Al ratio was determined to understand the aeolian input in the sediments (Pye and Krinsley, 1986; Haug et al., 2003; Roy et al., 2006, 2009, 2010; El-Asmar, 2023) as zircon concentrated in silt fractions. Total organic carbon (TOC %) have been determined from loss on ignition (LoI) using the method of Nelson and Sommers (1983) to know the paleo-vegetation cover of paleo-landscape.

The chemical Index of Alteration (CIA) is a widely used geochemical index to infer weathering intensity, source rock composition and paleoclimatic condition that calculates the extent of transformation of feldspar to clay minerals (Nesbitt and Young, 1982 1984; McLennan

et al., 1993; Fedo et al., 1995; Rieu et al., 2007; Roy et al., 2009; Yan et al., 2010; Perri, 2020; Mei et al., 2021; Wang et al., 2022). The CIA is calculated as;

$$CIA = [(Al_2O_3)/(Al_2O_3+CaO^*+K_2O + Na_2O) \times 100]$$

where oxides are in molar proportion and CaO* is the CaO contained in silicate minerals only (Nesbitt and Young, 1982) following the proposed method by McLennan et al. (1993).

The weathering conditions have been evaluated excluding K_2O known as Chemical Index of Weathering (CIW) also called CIA-K due to inconsistent behavior of K during pedogenesis (Harnois, 1988; Maynard, 1992). It is expressed as:

$$CIA\text{-}K = [(Al_2O_3 / Al_2O_3 + CaO + Na_2O) \times 100]$$

Sheldon et al. (2002) suggested a relation of the degree of chemical weathering with Mean Annual Precipitation (MAP) and Mean Annual Temperature (MAT) using major element geochemistry. Here MAP from K_2O free CIA is calculated as follows:

$$MAP\ (mm) = [14.265 \times (CIA\text{-}K) - 37.632]$$

where, $R^2 = 0.72$ with standard error of ±181 mm/yr.

Further MAT is determined by the following formula:

$$MAT\ (^\circ C) = -18.5S + 17.3.$$

where, S = salinization calculated by molecular ratio of ($K_2O + Na_2O/Al_2O_3$) and $R^2 = 0.37$ with standard error of ±4.4 °C.

In addition, more precise MAT estimation for Inceptisol paleosol only and applied to Quaternary paleosols from Hawaii (Sheldon, 2006c) is as follows:

$$MAT\ (^\circ C/yr.) = 46.9C + 4.0$$

where C= Clayeyness is calculated by a molecular ratio of Al/Si and $R^2 = 0.96$ with a stranded error of ±0.6 °C. Moreover, Nordt and Driese (2010) established more reliable climofunction for MAP estimation as,

$$MAP\ (mm/yr.) = 22.69(CALMAG) - 435.8,$$

Whereas, CALMAG (calcium-magnesium index) = $100 \times [Al_2O_3/(Al_2O_3 + CaO + MgO)]$ and oxides are in units of moles. The standard error for this relationship is ±108 mm.

4. Results and discussion

4.1. Paleosol profile

Paleosols and silty sand horizons have been recognized in two sedimentary succession designated as DD and KS section in two different localities (Fig. 2). Based on sedimentary and pedogenic characteristics, each of the study sections is divided into two major divisions as gray unit or newer alluvium unit (NA) and red unit or older alluvium unit (OA). In the DD section, the soil, paleosols (i.e., DMS, DGS-1 to DGS-4, DGS-5, and DGS-6) are alternated with the silty sand horizon (i.e., DS-1 to DS-4) as shown in Fig. 2a. Among the paleosols, DGS-5 and DGS-6 belong to the red unit/older alluvium (OA) unit whereas the rest are within the gray unit/newer alluvium (NA) unit. Paleosol DGS-5 has special importance due to its archaeological as well as paleo-settlement signatures (Fig. 4). Modern soils and paleosols from the KS section is designated as KMS and KGS-1 to KGS-4 respectively (Fig. 2b) Where KGS-2 to KGS-4 are paleosols of red unit/older alluvium (OA) unit.

4.2. Classification of soil/paleosols

Using the terminology of US soil taxonomic systems (Soil Survey Staff, 1999; Baillie, 2001) and field characteristics features, the studied soil/paleosol have been classified as very weak (Entisol), weak (Inceptisol), moderate (Aridisols), strong (Ultisol) and very strongly developed

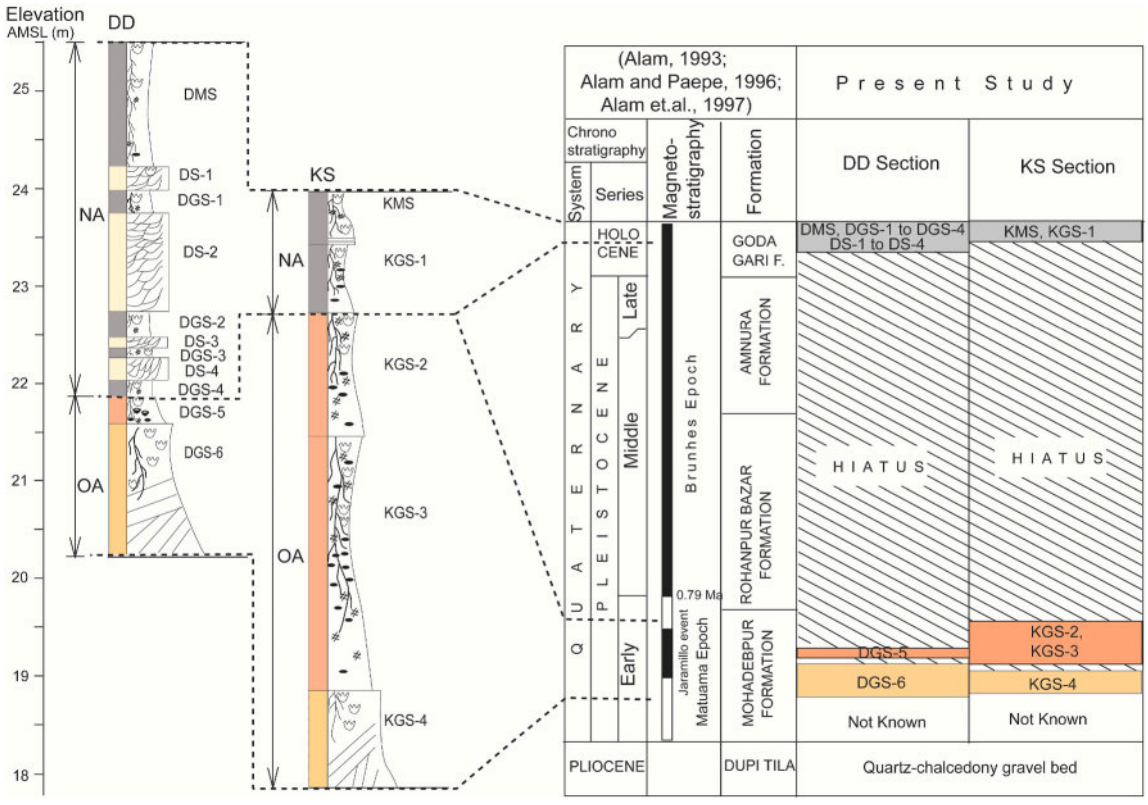

Fig. 3. Correlation between two studied sections (DD and KS Section) and their stratigraphic position established by comparing the stratigraphy after (Alam, 1993; Alam and Paepe, 1996; Alam et al., 1997).

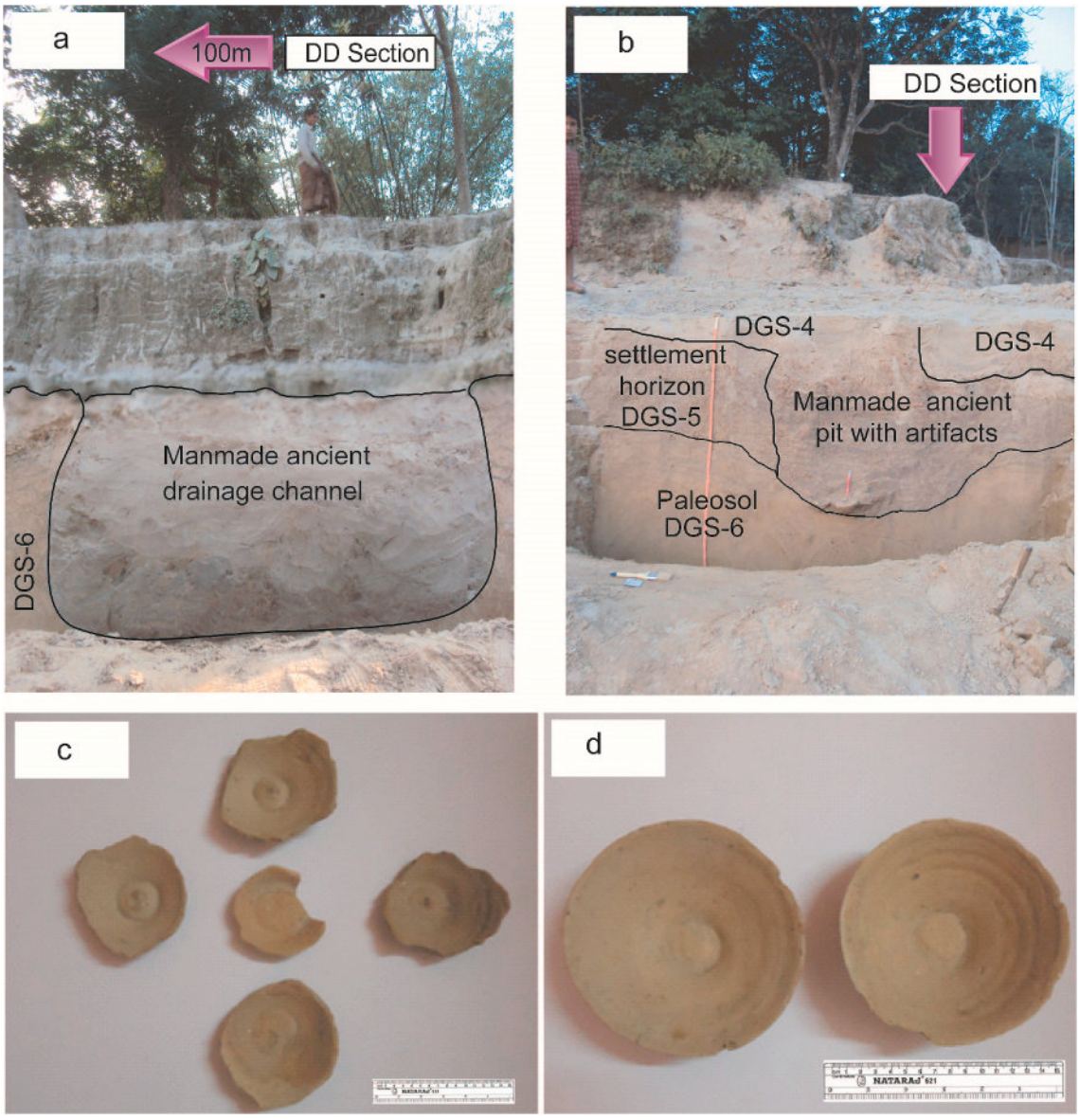

Fig. 4. Different geoarchaeological signatures found in and around DD section; (a) ancient man made drainage channel in southern wall of the excavation, 100 m east of DD section, in filled by secondary deposits; (b) pit at 10 m south of DD section, filled with ancient domestic waste, fragments of artifacts etc.; (c-d) potteries those were found at the lower part (paleo-settlement horizon/DGS-5) of DD section.

paleosol (Oxisols) (Table 1).

4.3. Paleosol chronology

The geologic age of the present studied paleosol sequences have been determined by correlation with paleomagnetic dated pedo-stratigraphy of the Barind Tract area (Alam, 1993; Alam and Paepe, 1996; Alam et al., 1997). Based on the lithostratigraphic position and signs of paleosol development, the studied red unit/older alluvium (OA) unit paleosols sequences are correlated to the Mohadebpur Formation which belongs to the Early Pleistocene age (Fig. 3). On the other hand the gray unit/newer alluvium (NA) unit paleosols and sediment sequences are correlated with Godagari Formation of Late Holocene age. Tentatively, dated artifacts recognized in the paleo-settlement horizon (Fig. 4) or the bottom of the gray unit stated that the age of Holocene deposits is about ~1300yr. BP – the time of the onset of cultural development of Somapura Mahavihara/Paharpur Buddhist Bihar. The artifacts studied, including earthen potteries (cups and dishes), were taken to the laboratory of the Department of Archaeology, Jahangirnagar University, Savar, Dhaka, Bangladesh where extensive collections of dated artifacts from various locations and periods, were used to compare our artifacts to determine the age of the artifacts (potteries) in rather relative method and tentatively dated approximately 1300 to 1200 years BP. It is to be noted that the artifacts (earthenware potteries, Fig. 4) found at the paleo-settlement horizons of the sedimentary succession are exactly similar those commonly found in Somapura Mahavihara (meaning 'large monastery') also known as Paharpur Buddhist Bihar archaeological site located at Noagoan district in northwestern part of Bangladesh. Charcoal samples from the artifacts containing horizon of the Somapara Mahavihara archaeological site has been well dated by C14 dating and found that Pala Dynasty predominantly occupied and ruled from about 770–810 CE (Alam et al., 2009). The thick sedimentary alluvial deposits analyzed in our study, which overlie past human settlements and are in close proximity SW to Somapura Mahavihara/Paharpur Buddhist Bihar. From the similarity view points of the potteries we can determine the age of paleo-settlement in rather relative method. Therefore, according to this assessment, the age of these artifacts ranges from approximately 1300 to 1200 years BP, corresponding to the mid-medieval period or the

Table 1
Classification of soil/paleosols studied at Durgadaha (DD) and Kujisahar (KS) section.

Soil type	Profile	Taxonomy (US soil taxonomy, 1999)	Color	Diagnostic field characters and geochemical properties
Very weakly developed paleosol	KMS and KGS-1	Entisol	Gray to light Gray (10 YR 6/1–7/1)	Silty clay to clayey textures, absence of diagnostic horizon, few mottling and root traces present, absence of Fe-Mn concretion, lower concentration of TOC%, very low chemical weathering and pedogenesis.
Weakly developed paleosol	DMS DGS1, DGS-2, DGS-3, and DGS-4	Inceptisol	Light gray to brownish gray (10 YR 8/1–7/1)	Silty clayey to clayey textures, poorly developed horizonization, few mottles and Fe-Mn concretion rootlets and animal barrows are present, with moderate TOC% and low chemical weathering and pedogenesis.
Moderately developed paleosol	KGS-4, and DGS-6	Aridisol	Light yellowish brown to brownish yellow (10 YR 6/4–6/6)	Clayey sand to silty sandy texture, well-defined horizonization, moderate to highly oxidized, root traces and animal barrows are common, few carbonate spots are recognizable, Fe/Mn concretion absent, low TOC%, chemical weathering (moderate CIA) and moderate to high pedogenesis
Strongly developed paleosol	KGS-2	Ultisol	Very pale Brown to brownish yellow (10 YR 6/3–6/8)	Silty clay to clayey texture, moderately defined horizonization, root traces and animal barrows are abundant in whole profile, clayey coating and Fe-Mn concretion are common, devoid of carbonate nodule, relatively moderate to higher TOC%, strong chemical weathering and pedogenesis and base loss ratio is >2.
Very strongly developed paleosol	KGS-3 and DGS-5	Oxisol	Light reddish brown to dark reddish brown (2.5 YR 6/4-3/4)	clayey to silty clayey texture, plenty of root traces and barrows, well-defined Bt and Bw/BC horizon, abundant root traces and animal barrows, clay coating along prismatic to columnar ped structures, carbonaceous coating, accumulation of sesquioxide (Fe/Mn concretion), pseudogleyed and devoid of carbonate nodules, relatively higher TOC%, extreme chemical weathering (higher CIA) and pedogenesis.

early Pala Dynasty. Further, this age has been confirmed by the study of climo-sequences correlating after the Asian monsoon strength of the last 1700 years (Morrill et al., 2003, Fig. 10).

4.4. Major element ratios

Different ratios calculated using major elements and have been plotted along with depth are shown in Fig. 5. From the figure, it is revealed that the average clayeyness (Al_2O_3/SiO_2) is relatively higher at B horizons of most of the paleosols and particularly the ratio is very high (0.23) in gray unit modern soil. Calculated salinization ($Na_2O + K_2O$)/Al_2O_3) are inverse characteristics relative to the clayeyness due to the removal of salts from B horizons. The estimated average salinization is minimal (0.25) in well-developed red unit silty clay paleosols and maximum (0.51) in red unit sandy clay paleosols. It is 0.36 in both gray unit modern soil and paleosols. Base losses ($Al_2O_3/Na_2O + K_2O + CaO + MgO$) are increased in highly weathered red unit silty clay paleosols but depleted in gray unit silty sand sediments. This ratio is comparatively high in Bt/Bw horizon among all the paleosols. The mean base loss of red unit silty clay and sandy clay paleosol is 2.29 and 1.5 respectively, while it is 1.4 and 1.08 for gray unit modern soil and paleosols and silty sand sediments respectively. Mean calcification ($CaO + MgO/Al_2O_3$) is low (0.22) in red unit silty clay paleosols and higher (0.50) in gray unit silty sand sediments. This value is found to be moderate in gray unit modern soil and paleosols and also in red unit sandy paleosols. Mean calcification variations along the vertical profile (Fig. 5) also signify that the Ca and Mg were removed from Bt/Bw horizon of red unit silty clay paleosols and gray unit modern soil. However, these elements are accumulated in Bt horizon of red unit sandy clay paleosols. Major element composition can be used to evaluate the nature of the source rock composition. The discriminant functions (F1-F2) of Roser and Korsch (1988) separate four major provenance: mafic (P1), intermediate (P2), felsic (P3) and quartzose recycled (P4), based on the abundances of seven elements. On the discriminant function diagram the DD and KS sediments nearly all fall within the quartzose sedimentary (P4) field (Fig. 7). The data extend from the boundary with P3 (felsic) to P4 (quartzose sedimentary) field. Few samples are plotted on the boundary of P3-P4 field due to the lower concentration CaO and Na2O. The overall position and trend of the sediments in the F1-F2 diagram suggest that almost all the samples (soil, paleosols and silty sand) were derived from similar felsic-quartzose recycled types of source composition.

Chemical Index of Alteration (CIA) and Chemical Index of Weathering (CIW) show strong correlations within both modern soils and paleosols in both sections (Figs. 5 and 6). Sediments experienced extensive weathering shows high value of CIA (80–100), moderate (70–80) and minimal weathering (50–70) (Nesbitt and Young, 1982). Relative strength of CIA and CIW indexes signifies that red unit silty clay paleosols are products of extreme weathering during pedogenesis. Among the red units, particularly the Bt and Bw horizons of paleosol

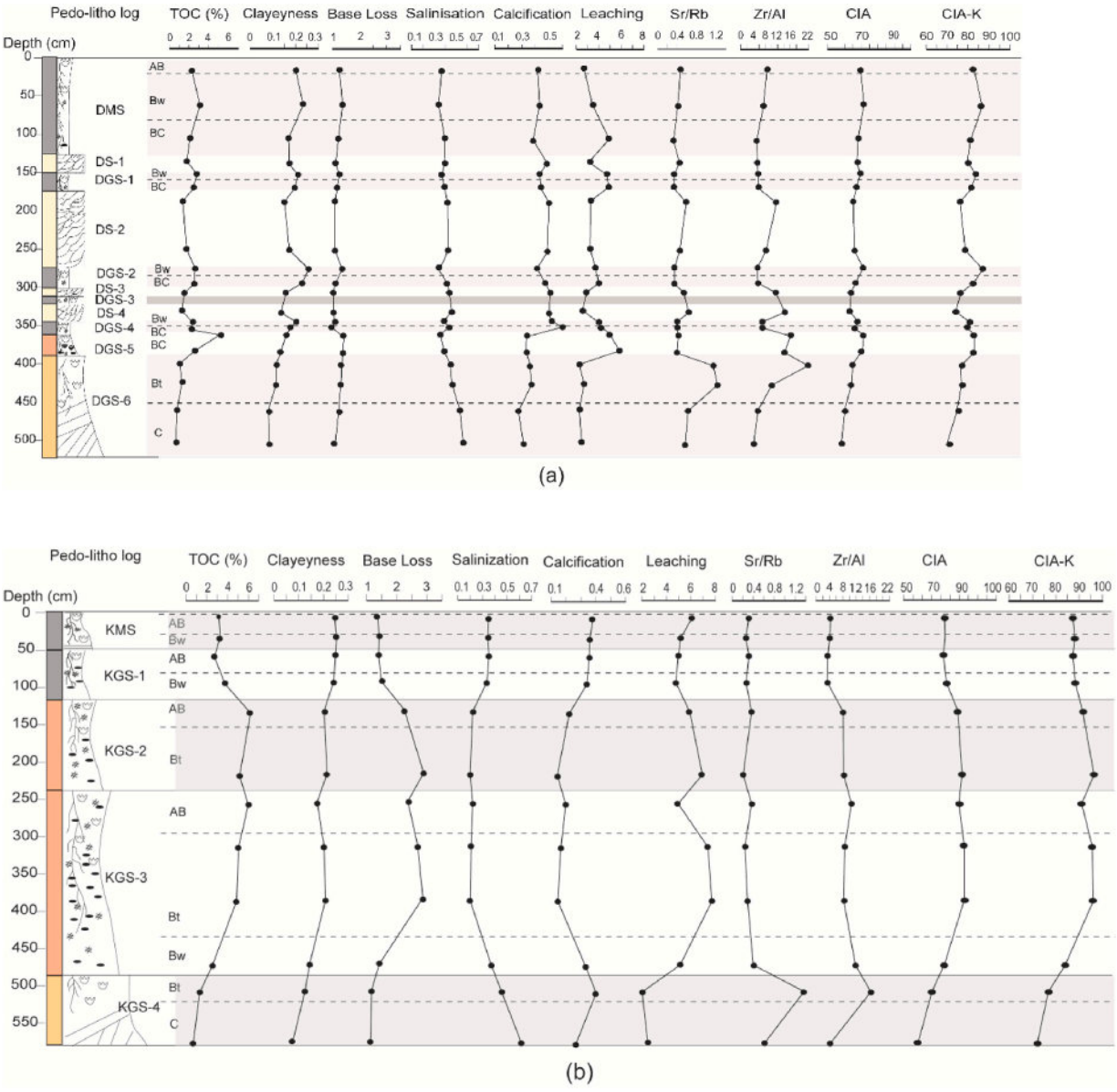

Fig. 5. TOC and molecular ratios of weathering and pedogenic indices variations with respect to various soils/paleosols with different horizons (i.e., AB, Bw, Bt, BC and C horizons) and sediment units of (a) DD section and (b) KS section. Bt: An argillic horizon where clay accumulation is evident. AB: A transitional horizon between A and B horizons, displaying characteristics of both. C: The parent material horizon, relatively unaltered by soil formation processes. Bw: A weakly developed B horizon, indicating initial stages of soil development.

KGS-3 show relatively highest value of CIA and also higher CIW respectively. Significant results were obtained also from red unit sandy paleosols. The observed values of both CIA and CIW from the poorly altered parent horizon (C) and Bt horizon indicates deviations (Fig. 5) representing moderate to strong weathering conditions due to the presence of unaltered labile element such as Na2O (1.42 and 1.49 wt%). In the paleosol DGS-5, this index shows a similar pattern of the lower-most of paleosol KGS-3 which represents Bw horizon. Average CIA and CIW values are 70.7 and 88.2 in gray unit modern soil and paleosols respectively (Table 2). Deviation of both indexes from A and Bw horizon is 5 units in DMS modern soil which signifies moderate to weak weathering during pedogenesis. Weak weathering during pedogenesis is observed in gray unit paleosols. In these paleosols, CIA and CIW are 70. and 86.8 for paleosol DGS-1, 71.5, and 89.9 for DGS-2 and in paleosol DGS-4 those indexes are 67.8 and 84.2 respectively. Among these paleosols, weathering, and pedogenesis are minimal in DGS-4. The average CIA and CIW are 61.6 and 77.0 attained from gray unit silty sand horizons (DS-1 to DS-4) indicates low weathering at their sources.

4.5. Trace element ratios

Ba/Sr ratios are valuable tracer for understanding the leaching condition in soil and paleosols. Ba/Sr ratios have been calculated and plotted against depth to understand leaching conditions (Fig. 5). From this figure, lower value of Ba/Sr ratio is observed at the top of all paleosol profiles and an increasing trend towards the bottom. Among all paleosols, KGS-3 is heavily leached and the ratio is 4.96 at the top (AB horizon) and it is 7.74 and 5.12 at the lowermost portion of Bt and BC horizon respectively. Paleosol KGS-2 represents also a moderate to high Ba/Sr ratio, i.e., 5.91 and 6.96 at the topmost AB and lowermost Bt horizon respectively. Minimal leaching (avg. 2.37) is found in red unit sandy paleosols. In these paleosols, the ratio Ba/Sr is 2.24 and 2.49 at the Bt and C horizons of paleosol DGS-6 respectively. Higher value at the C horizon of this paleosol can be due to leaching out from the upper

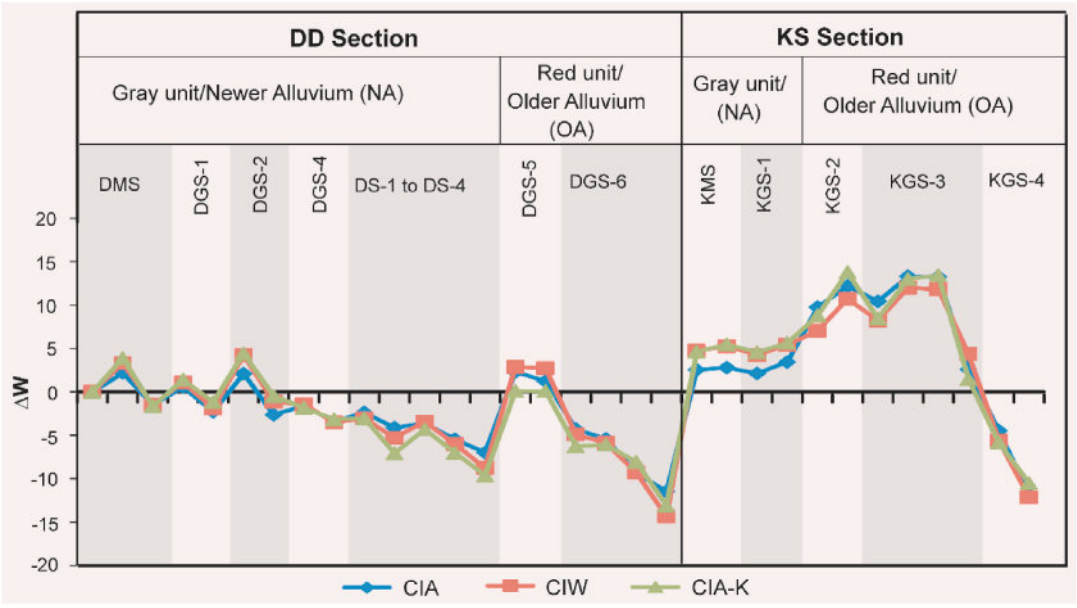

Fig. 6. Deviation of weathering (ΔW) (Sheldon and Tabor, 2009) indices CIA, CIW and CIA-K represent the comparative intensity of weathering among various soil, paleosols and silty sandy sediments horizons in two sections.

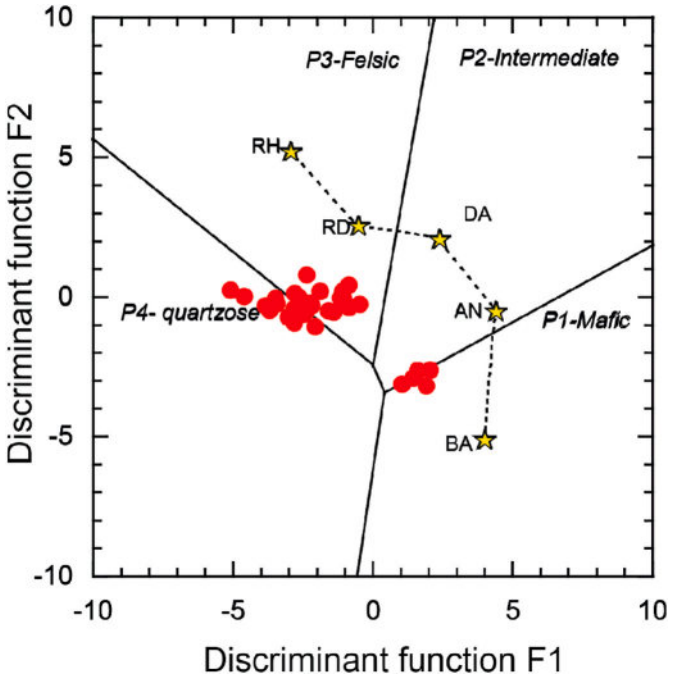

Fig. 7. Major element provenance discriminant plot for soil, paleosols and sediments of DD and KS section (Roser and Korsch, 1988). P1-mafic igneous; P1-mafic igneous; P2-intermediate igneous; P3-acid igneous and P4-quartzose detritus recycled sedimentary Stars: BA, AN, DA, RD, RH – average basalt, andesite, dacite, rhyodacite and rhyolite, as plotted by Roser and Korsch (1988).

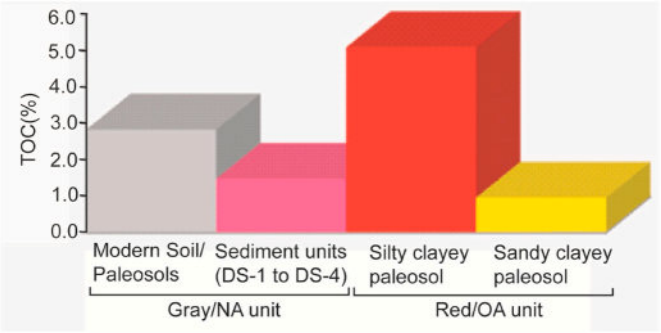

Fig. 8. Comparison of average TOC (%) concentration among the different soil/ paleosols and sediment units.

sandy Bt horizon. Paleosol KGS-4 also represents similar ratios. Moderate to low leaching (2.65–4.92) is observed in DMS modern soils. Other gray unit paleosols (DGS-1, DGS-2, and DGS-4) also signify moderate to low (avg. 4.26) leaching intensity. Among these paleosols, a difference in the ratio between Bw and BC horizon is high in DGS-2 paleosols indicating relatively more leached paleosol.

Sr/Rb ratios are important for understanding the leaching condition in soil and paleosols. The ratio Sr/Rb is relatively lower at the top of the profile and increasing toward parent (C) horizons. The highest ratio observed in the upper part (Bt horizon) of paleosol DGS-6 and KGS-4 (Fig. 5) i.e. presence of higher amount of Sr and less leaching, relatively low weathering indicates arid condition.

The ratio is 1.14 and 1.37 at the upper part of these paleosols, whereas, it is 0.56 and 0.61 at the parent horizons respectively. The ratio is relatively low due to less concentration of Sr, in all other paleosols and modern soils that varies from (top to bottom) 0.37–0.40 in paleosol KGS-3, 0.37-0.21 in KGS-2, 0.32-0.27 in KGS-1, 0.34-0.33 in DGS-1, 0.34–0.35 in DGS-2, 0.4 in DGS-4, 0.32-0.26 in KMS, 0.47-0.32 in DMS modern soil and 0.5–0.7 in silty sand sediment horizon (DS-1 to DS-4) respectively (Fig. 5). These results especially represents that the ratio is almost followed the similar trend from the top (Bw horizon) to bottom ((BC horizon) of paleosols DGS-1 and DGS-2. This result represents relatively low concentration of Sr, high leaching and high CIA thus indicates humid climatic conditions condition.

Certain elemental ratio such as Zr/Al has been successfully used as a proxy for the source of Aeolian input (Rodrigo-Gámiz et al., 2015). Significant results were also obtained from the ratio of Zr/Al. In the red unit sandy paleosol (DGS-6 and KGS-4), the ratio varies from 21.63-4.27 (from top to bottom) with an average value of 10.38 (Fig. 5). Higher ratio of Zr/Al as well as high concentration of Zr at the top of the profile relative to parent horizon strongly suggests aeolian input during

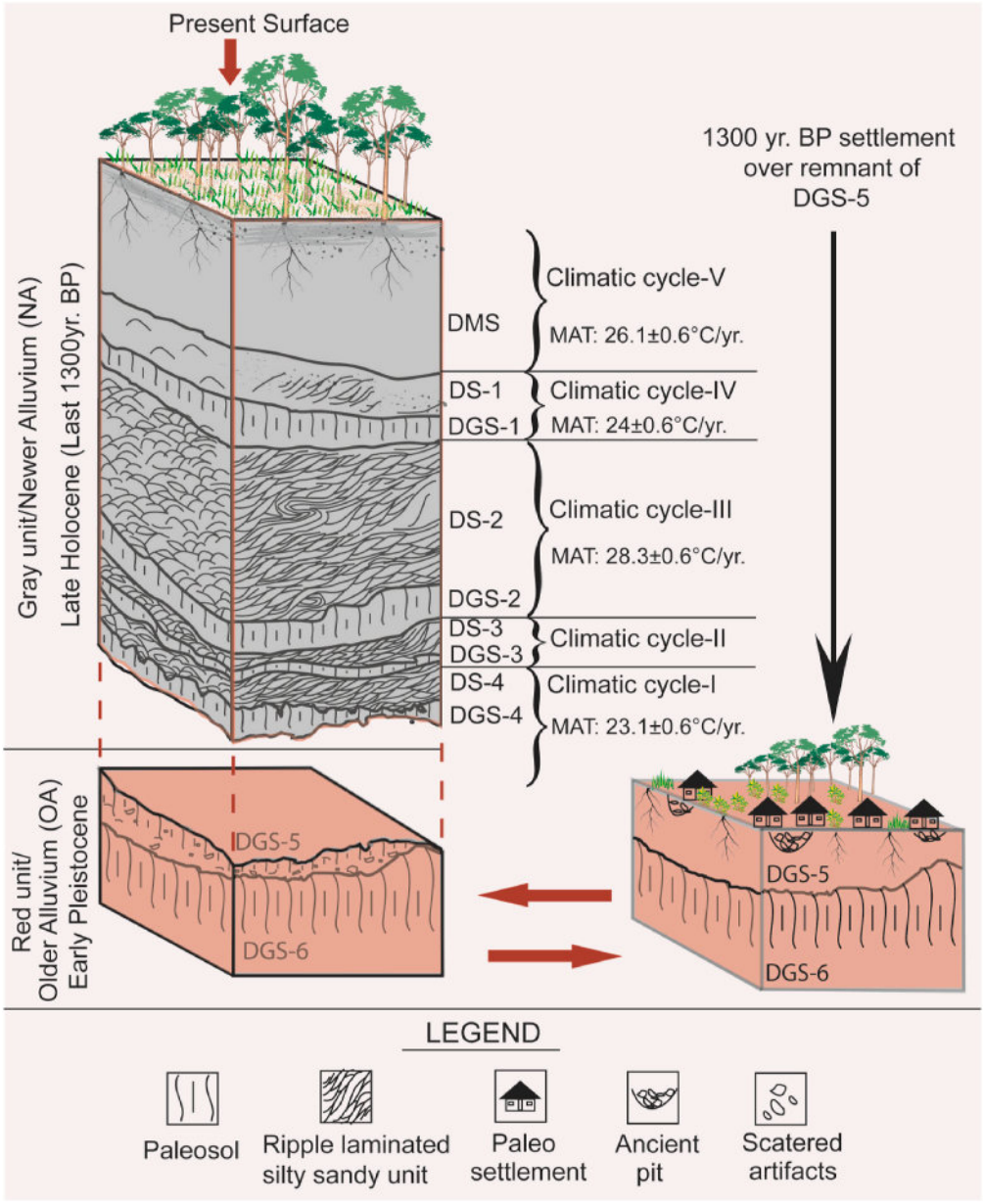

Fig. 9. Schematic diagram showing reconstruction of paleo-settlement (right) over the Pleistocene red unit paleosol DGS-5 and consecutive deposition and development of paleosols and modern soils at the top within five short term climatic cycles in Late Holocene (last ~1300yr.) time.

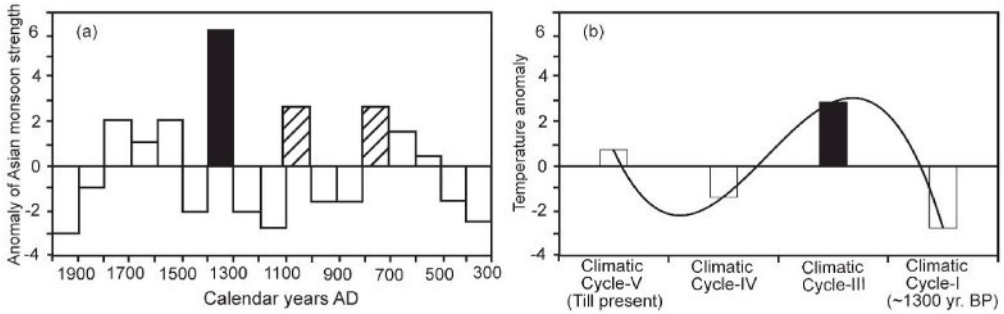

Fig. 10. (a) Abrupt changes in monsoon strength observed in the Asian monsoon region for historical time periods (Morrill et al., 2003), where positive and negative anomaly represents strengthening of monsoon (warm) and weakened monsoon (cool) episodes respectively; (b) Anomaly of MAT changes through five climatic cycles during ~1300 years. BP (archaeological dating) of the study area. No conclusion can be drawn about climatic cycle-II due to lack of data. The black shaded positive anomaly at cycle-III represents medieval warm period (MWP) that can be correlated to the anomaly of monsoon strength indicated ~1300AD of figure-a and IV can be correlated to LIA events.

Table 2
Oxides of major and trace elements with LOI in wt% and CIA, CIW and CIA-K along different horizons of soil and paleosol profiles and sediment units in two studied sections.

Soil/Paleosol	Sample No.	Horizon	SiO_2	TiO_2	Al_2O_3	Fe_2O_3	MnO	MgO	CaO	Na_2O	K_2O	P_2O_5	Ba	Sr	Rb	Zr	LOI	Total	CIA	CIW	CIA-K
DMS	DD1	AB	57.66	0.83	19.64	7.39	0.09	2.42	1.30	1.07	4.96	0.14	476	115	240	281	3.95	99.63	69.44	85.72	82.64
	DD2	Bw	53.78	0.86	21.54	7.97	0.09	2.55	1.01	0.92	5.42	0.11	614	114	269	262	5.31	99.78	71.65	89.01	86.53
	DD3	BC	61.62	0.70	17.81	6.32	0.07	2.06	1.22	1.19	4.68	0.14	741	96	291	198	3.68	99.69	67.95	84.22	81.00
DS1	DD4	–	60.65	0.76	18.18	6.60	0.08	2.49	1.40	1.29	4.72	0.14	557	112	246	177	3.06	99.52	70.03	86.81	84.04
DGS1	DD5	Bw	55.86	0.90	20.18	7.61	0.08	2.58	1.15	1.06	5.15	0.13	725	97	281	201	4.91	99.80	67.18	83.81	81.48
	DD6	BC	56.77	0.87	19.20	7.45	0.07	2.32	1.45	1.10	5.34	0.11	732	95	277	202	4.32	99.00	71.56	89.95	87.07
DS2	DD7	–	64.27	0.77	16.59	5.96	0.08	2.03	1.71	1.37	4.40	0.22	673	131	219	341	2.11	99.70	66.84	84.58	82.17
	DD8	–	60.58	0.81	17.46	7.32	0.09	2.28	1.51	1.26	4.90	0.18	603	120	258	259	3.04	99.63	67.88	84.27	80.82
DGS2	DD9	Bw	51.69	0.95	22.75	8.59	0.10	2.90	1.11	0.82	6.01	0.14	619	107	307	221	4.48	99.77	66.04	82.21	79.49
	DD10	BC	53.53	0.88	21.00	7.88	0.08	2.98	1.33	1.30	6.09	0.12	653	104	289	218	4.30	99.49	67.09	82.66	79.59
DS3	DD11	–	62.94	0.75	16.63	6.27	0.10	2.13	1.70	1.38	4.72	0.18	615	135	247	332	2.58	99.60	65.35	80.43	75.58
DS4	DD12	–	66.39	0.65	15.12	5.73	0.08	1.73	1.75	1.46	4.21	0.17	528	133	203	387	1.98	99.46	65.84	82.28	78.33
DGS4	DD13	Bw	56.47	0.88	19.53	7.48	0.08	3.03	1.43	1.24	5.17	0.16	692	109	266	242	4.03	99.73	64.01	79.68	75.63
	DD14	BC	58.67	0.85	17.91	7.11	0.07	3.10	1.61	1.32	5.21	0.13	699	107	263	241	3.93	99.91	62.47	76.95	73.03
DGS5	DD15	BC	59.85	0.72	16.20	5.81	0.13	1.45	1.00	0.94	3.96	0.21	719	93	216	469	9.20	99.62	71.76	88.58	82.75
	DD16	BC	66.15	0.64	15.48	5.07	0.26	1.42	0.85	1.03	4.06	0.20	821	90	226	389	4.20	99.55	70.70	88.43	82.73
DGS6	DD17	Bt	70.18	0.55	13.80	4.99	0.08	1.11	1.20	1.26	3.78	0.16	545	155	133	534	2.14	99.48	65.19	80.80	76.38
	DD18	Bt	71.16	0.47	13.89	4.30	0.11	1.18	1.17	1.29	3.96	0.12	692	165	131	250	1.79	99.62	64.05	79.85	76.56
	DD19	BC	77.80	0.24	11.01	2.90	0.07	0.52	0.97	1.21	3.60	0.06	425	119	188	111	1.19	99.63	60.17	76.43	74.59
	DD20	BC	77.33	0.27	10.42	3.41	0.07	0.56	1.13	1.53	3.12	0.06	430	110	192	80	1.31	99.35	57.98	71.37	69.56
KMS	KS1	AB	52.68	0.91	22.00	8.09	0.10	2.63	0.97	0.88	5.75	0.14	997	104	320	169	5.48	99.86	72.00	90.43	87.29
	KS2	Bw	52.23	0.97	22.33	8.09	0.08	2.50	0.92	0.82	5.87	0.13	757	93	347	161	5.59	99.74	72.26	90.96	88.12
KGS1	KS3	AB	52.96	0.96	22.37	8.10	0.08	2.43	1.04	0.85	5.90	0.13	829	106	326	142	4.78	99.82	71.59	89.99	87.22
	KS4	Bw	52.65	0.94	21.61	8.35	0.10	2.27	0.86	0.80	5.48	0.13	686	92	333	133	6.51	99.86	72.90	91.12	88.27
KGS2	KS5	AB	54.81	0.93	18.87	8.43	0.28	1.22	0.59	0.42	3.22	0.04	699	76	200	273	10.64	99.68	79.21	92.77	91.45
	KS6	Bt	56.35	0.90	20.57	7.70	0.08	0.98	0.25	0.18	3.57	0.12	521	48	221	304	8.87	99.75	81.65	96.42	96.42
KGS3	KS7	AB	58.35	0.91	17.48	7.49	0.06	0.93	0.64	0.32	3.03	0.03	578	74	196	331	10.27	99.72	79.89	93.95	91.11
	KS8	Bt	57.62	0.84	19.74	7.26	0.09	1.10	0.25	0.27	3.36	0.07	563	49	194	304	8.73	99.53	82.78	97.68	95.64
	KS9	Bt	57.55	0.89	20.29	7.15	0.20	1.01	0.24	0.24	3.44	0.05	732	60	202	302	8.45	99.72	82.73	97.53	96.08
	KS10	BC	65.34	0.68	16.00	5.32	0.15	1.47	0.86	0.89	4.11	0.21	759	95	230	336	4.36	99.60	72.06	90.08	84.11
KGS4	KS11	Bt	69.21	0.56	14.65	4.46	0.07	1.50	1.15	1.42	3.93	0.13	527	167	119	430	2.33	99.61	64.99	80.11	76.81
	KS12	BC	79.07	0.15	10.11	2.51	0.04	0.49	0.80	1.49	3.50	0.04	424	108	174	78	1.23	99.53	57.67	73.57	72.16

pedogenesis. This ratio is relatively moderate (avg.9.82) in paleosol KGS-3 and low (avg.8.47) at Bt horizon due to the enrichment of Al_2O_3. The average ratio of Zr/Al is 8.16 in paleosol KGS-2 indicates more or less uniform concentration of Zr/Al. The average ratioof Zr/Al in KGS-1 and KMS is 3.82 which indicates minimal among all soil, paleosol, and silty sandy sediment horizons due to the enrichment of clayey deposits. Average ratios 7.15 and 10.14 are obtained from DMS and silty sandy sediment horizons respectively. In the DMS, the Zr/Al vale shows low (5.15) at a more weathered Bw horizon relative to the AB and BC horizon.

4.6. Abundance of total organic carbon (TOC)

Total organic carbon (TOC) has been plotted against different paleosols, modern soils, and sediment horizons (Figs. 5 and 8). These figures show variations of TOC (%) values in paleosols and sediment units. A higher proportion of TOC is observed in well-developed paleosols than in the parent sediments (C horizon). Abundances of TOC% (avg.) is maximum (>5%) in red unit silty clay paleosols (DGS-5, KGS-2, and KGS-3) and minimum in red unit sandy clay paleosols (DGS-6 and KGS-4). However, TOC content in gray unit paleosols and silty sand horizon is (~3%) and (1.5%) respectively.

The higher TOC % in the silty clay layer compared to the modern soil layer. The concentration of TOC% signify that higher pedogenic horizon (Bt horizon) or well developed paleosol horizons provides higher TOC percentage than the weakly developed paleosol (Less developed AB/Bw horizon). Therefore the modern soil contain moderate to low total organic carbon (TOC). The causes of low concentration of TOC in sandy parental horizon is due to their unaltered state with no or little pedogenic activities, although they show some organic carbon content which were concentrated by bacterial activities during the time of their deposition.

4.7. Applicability of climo-functions

Climo-functions are used to estimate the mean annual temperature (MAT) and mean annual precipitation (MAP) using geochemical composition from the Bt and Bw horizons of paleosols (Sheldon et al., 2002; Sheldon, 2006a; Retallack, 2004; Stinchcomb et al., 2016; Gillot et al., 2022). For the estimation of MAP after Sheldon et al. (2002), the present geochemical studies of various paleosols and modern soils are considered to be suitable for understanding climo-functions. CIA-K index for different horizons of various soil/paleosols are presented in Table 2. The topography and morphologic positions of these paleosols are also fitted to the standard criteria after Sheldon et al. (2002).

4.8. Paleo-environment and climate

Paleo-environment and paleo-climate of the study area have been reconstructed based on the interpretation of lithology, paleosols, geo-archaeological evidence and geochemical indices with climo-functions. From chronological correlation and archaeological dating, the Quaternary deposits of the study area are considered to be of Early Pleistocene and Late Holocene age. The Holocene age of the deposits can be considered 1300 years BP as evident from the artifact interpretation as well as paleo-settlement history. The thickness of Holocene age sediments in the study area is 350 cm. High sedimentation rates in the study area by a dense network of rivers originating from the Himalayan mountain range. These rivers transport significant amounts of sediment from the Himalaya, making it feasible for a 350 cm thick sediments deposition within 1300 years. Beside these, development of South Asian Monsoon (SAM) intensified the erosion in the Himalayan region which carried enormous amount of sediments to the Bengal basin. According to the recent work by Haque and Hoyangi (2021) estimated the average sedimentation rate of the Bengal basin is approximately 1.96–2.89 mm/yr. According to the sedimentation rate (highest~2.89), the deposited thickness of the sediments would have been 375.7 cm/1300 year in the study area. Even though considering the compaction of the sediments and break of sedimentation would justify the deposition of the 350 cm sediment thickness by 1300 years in the study area.

The Early Pleistocene deposits are older and are discussed as a red unit or older alluvium unit (OA) and Holocene deposits are discussed as gray units or newer alluvium units (NA).

4.8.1. Early Pleistocene environment and climate

The global climate in the Pleistocene epoch was influenced by several glacial (dry and cold) and interglacial (warm and humid) events (Goñi, 2022; Hughes et al., 2006; Hughes and Gibbard, 2018; Sánchez-Bandera et al., 2023). These climatic changes have been evidenced by worldwide continental and deep sea environment signatures (Alam, 1993; Groot, 1991; Froese et al., 2000; Heine and Völkel, 2010; Rohling et al., 2021). In the present study climatic fluctuations during Early Pleistocene have been recognized from geochemistry and field characteristics of three different paleosols.

The sediments of moderately developed aridisol-like paleosol (DGS-6 and KGS-4) of sandy texture with cross-bedding structures (Fig. 2) at the lowermost portion suggest channel deposition. These coarser sandy deposits are the results of high hydrodynamic regimes of deglaciated water originated from melted glacier of Himalayan region under hot and humid events of interglacial periods. Further, the climate was dramatically shifted to drier phases after the deposition of these sandy deposits. Weathering and pedogenesis acted on such paleosols under cold and arid to sub-humid climates where MAP: 1000 ± 181 mm/year and MAT: 9 ± 4.4 °C/year (using formula after Sheldon et al., 2002; Kogler and Hembree, 2019; Ghasera and Rashid, 2024) with medium to high oxidizing environment.

These paleosols (i.e. DGS-6 and KGS-4) represent higher calcification and salinization at Bt horizon and comparatively lower clayeyness and base loss and also medium to low CIA, CIW values than other red unit paleosols support the cold and arid to sub-humid climate (Fig. 5a and b). Moderate leaching associated with scarcity of water inhibited depletion of Sr from the sediments. Also, the concentration of Zr with a higher ratio of Zr/Al indicates aeolian input. Low TOC content, yellow to brownish yellow color and nonexistence of Fe-Mn concretions also recommend the aforesaid climate. Alam and Paepe (1996) also reported similar aridisol-like paleosol was developed in the Barind area, NW Bangladesh under a semi-arid to arid climate in the Early Pleistocene age. Clay mineral analysis of red clay deposits from the Central Carpathian Basin (Hungary) reported that the lower part of the early Pleistocene climate was cold and arid to semi-arid characteristics (Almogi-Labin, 2011). Heine and Völkel (2010) also analyzed soil clay minerals in Namibia (Africa) and documented that the climate that prevailed during the early period of the lower Pleistocene was arid to semi-arid.

Sedimentological properties of strongly developed red unit silty clay paleosols (KGS-3, DGS-5) ensure that these are fluvial deposits. Relatively moderate to poorly weathered clayey silt-rich Bw horizons suggest that the sediments of these paleosols were originally deposited as clayey silt to silty sand under moderate to high hydrodynamic energy. Overall pedo-sedimentological and geochemical analyses stated that the present clay-rich red products are the results of extreme weathering and pedogenic interactions under oxidizing environments. Paleosol developed in these sitly sand deposits under relatively hot and humid climatic conditions in Early Pleistocene time (Table 3). However, temperature and precipitation were much lower relative to the present conditions of the area. The calculated MAP that prevailed during the development of these paleosols is 1461 ± 181 mm/year (Sheldon et al., 2002) and 1527 ± 108 mm/yr (Nordt and Driese, 2010) and MAT is 14 ± 4.4 °C/yr (Sheldon et al., 2002). Moreover, these paleosols show moderate clayeyness, lowest salinization, lower Sr/Rb ratio and lower calcification along with the highest base loss and leaching relative to other red unit paleosols indicates sub-humid climatic condition. Other properties

Table 3
Estimated MAT and MAP with paleoclimatic assessment of different climatic cycles of the studied soil, paleosols and sediment units.

Paleosol/ Sediment Units	Types of Paleosol	Mean Annual Temperature (MAT °C/yr.)	Mean Annual Precipitation (MAP mm/yr.)	Relative Assessment of Paleoclimate	Climatic Cycle	Geologic Age
DMS	Inceptisol	26.1 ± 0.6	–	Hot and humid	V	**Late Holocene (Last ~1300 years BP)**
DS-1	–	–	–	More humid.	IV	
DGS-1	Inceptisol	24 ± 0.6	–	Cold, semi-arid to sub-humid.		
DS-2	–	–	–	More humid.	III	
DGS-2	Inceptisol	28.3 ± 0.6	–	Very hot, humid to sub-humid.		
DS-3	–	–	–	More humid	II	
DGS-3	Inceptisol	–	–	Semi-arid to sub-humid		
DS-4	–	–	–	More humid.	I	
DGS-4	Inceptisol	23.1 ± 0.6	–	Cold, semi-arid to sub-humid.		
Paleo-settlement period			–	Cold, dry and arid.		
KGS-2	Ultisol	14 ± 4.4	1478 ± 181[a] 1550 ± 108[b]	Cold, humid to Sub-humid.	I	**Early Pleistocene**
KGS-3	Oxisol	14 ± 4.4	1461 ± 181[a] 1527 ± 108[b]	Cold, humid to Sub-humid.		
DGS-6 and KGS-4	Aridisol	9 ± 4.4	1000 ± 181	Cold, semi-arid to sub-humid		

[a] Formula after Sheldon et al. (2002).
[b] Formula after Nordt & Driese (2010).

like reddish brown to dark reddish brown color, abundances of root traces, moderate concentration of Fe-Mn concretions and nonappearance of calcium carbonate nodules in these paleosols support the estimated MAP and MAT. It is significant that estimated paleo-temperature and precipitation were gradually increased from the immediate earlier conditions. However, degree of paleosol development and relatively higher TOC concentration indicate the existence of this climatic phase for a long period.

Alam and Paepe (1996) recognized strongly developed paleosol GS21 above the aridisol (GS25) in the Barind area which was developed under a hot and humid climate in the Early Pleistocene. The paleosol GS21 may correlate to the studied strongly developed paleosol which also indicate the consistency of estimated MAP and MAT as well as climate systems.

Depositional, pedogenic, and biogenic features indicate minor climatic differences between the paleosols KGS-3 and KGS-2. The climate was steady for a long time during the formation of the paleosol KGS-3. Afterward, the MAT and MAP were progressively increased and the climate became relatively more hot and humid. Therefore, the depositional basin has been over flooded than earlier conditions. Paleosol KGS-2 is considered cumulative in nature formed progressively with the increment of a few millimeters or a centimeter of sediment per year by numerous floods on the surface of paleosols KGS-3. The clayeyness is highest among red unit paleosols which also signifies a predominant of fine grain texture. Relative abundance of TOC is consistent with humid and hot climate than the previous one. However, it is difficult to apply climofunctions to a cumulative nature of palaeosols to estimate the paleo-MAP and MAT. Although the estimated MAP and MAT from climofunction are observed as MAP: 1478 ± 181 mm/year (Sheldon et al., 2002) and 1550 ± 108 mm/year (Nordt and Driese, 2010) and MAT: 14 ± 4.4 °C/year (Sheldon et al., 2002). From the above observation, it is quite evident that during the early Pleistocene time, two climatic phases are noticeable i.e., a dry cool and sub-humid climate followed by the relatively hot humid climate in the Joypurhat District of the north-western part of Bangladesh.

4.8.2. Late Holocene (Last ~1300 yr) environment and climate

After the end of the Last Glacial Maximum, approximately around 11.7 k years BP, the climatic trend shifted towards wetter phases. Subsequently, several fluctuations occurred in the Holocene climatic history, from around 10 k years BP to the present (Alam et al., 1997; Chauhan and Sharma, 2000; Wang et al., 2005, 2008; Alam et al., 2009; Kotlia and Joshi, 2013). These climatic fluctuations play a crucial role in the formation of various landforms and river valleys. The past human settlements were built on these valleys or riversides that ensure water availability during drier periods or droughts. However, they built settlements on relatively elevated landmass when the climatic phase was warm and more humid to protect themselves from devastating floods. In extreme humid climatic events, these past settlements on valleys experienced several devastating floods and were wrapped by sedimentations. These signatures were also recognized in the present study area especially in DD section (Fig. 4). Alternating deposits of modern soil (DMS) with four silty clay to clay paleosols (DGS-1 to DGS-4) and four silty sand horizons (DS-1 to DS-4) within the gray unit/newer alluvium (NA) unit in DD section suggest effects of several consecutive low and high flood episodes as well as alternation of five short term climatic cycles.

4.8.2.1. Climatic cycle I. Before ~1300 years, the area was experienced by large erosional processes and created several valleys/terrace like morphological features. In episode 1, at the time of ~1300 yr. BP, peoples made their settlements on the eroded surface of early Pleistocene deposits or low land that represents the paleosol surface DGS-5 (Fig. 9). At that time the river water level was most probably lowered as the settlement area was not flooded. However, lower level of river water signifies a lower sea level and/or drier climate as well as lower rate of precipitation. Over the paleo-settlement surface, artificial or man-made drainage channels for water transportation from nearby river channels suggest demand for excess water for agricultural and domestic uses that support the area was not inundated by floods as well as stabilized in dry and arid climatic episodes. Signatures of dryness or aridity are also obtained from geochemical evidences. It is important to note that paleosol DGS-5 is correlated with Bw horizon of the same paleosol KGS-3. Comparison of paleosol DGS-5 and KGS-3 provides relatively higher amounts of Zr and higher Sr/Rb in Bw horizon of DGS-5, which significantly represents that paleo-settlement surface received aeolian dust in extremely dry conditions.

During the period of paleo-settlement, climate was dry and later the aridity reached its maximum level. Therefore, highest dryness (set of

droughts) and scarcity of water might be the key factors for the abandonment or demise of these settlements. The in-situ position of settlement signatures (i.e. artifacts, pits, manmade channels) and geochemical data of DGS-5 strongly suggest maximum dryness (drought) was the prime cause of abandonment of past settlements than other favorable causes (i.e. flood, earthquake, etc.).

A study of phytolith analysis of archaeological soils from the neighboring Somapura Mahavihara site in the Paharpur area is also supportive of the dryer climatic condition (Alam et al., 2009). This study confirmed that cool and dry conditions persisted around Paharpur and the surrounding regions throughout the period from 730 CE–850. Pollen analysis of sediments from the Deorital area, Inner Lesser Garhwal Himalaya also suggested the climatic deterioration between ca. 2.0 and 1.4 ka BP (Chauhan and Sharma, 2000). Rühland et al. (2006) suggested that the drier climatic conditions prevailed in the Pinder valley around 1.6 ka BP. Pollen data obtained from the Spiti region also specify cool/dry conditions between ~ 2.0 and 1.0 ka BP (Mazari et al., 1995). Geochemical records of a 3.55 m long lake sediment core from the Badanital Lake (Garhwal Himalaya, India) also reveal drier and semi-arid to arid climate with reduced rainfall existed at around 1.8 Ka −920 yr BP (Kotlia and Joshi, 2013).

After the abandonment of past human settlements in the study area, climatic aridity was gradually shifted to relatively wetter/humid events and it is more likely the area was again inundated by numerous low-energy floods that reflected in the depositional sequences. Therefore, the settlement horizon was covered by fine grain sediment and pedogenic processes operated to form the weakly developed Inceptisol like paleosol DGS-4 (Figs. 2 and 9). Geochemical climofunction stated that the paleosol DGS-4 was developed under 23.1 ± 0.6 °C/yr. MAT (using formula after Sheldon, 2006c) (Fig. 9 and Table 3), which is logically warmer than previous cold and arid climates. However, it was 2–3 °C cooler than the present MAT systems. The relative magnitude of chemical weathering (CIA, and CIW) and other geochemical proxies suggests this paleosol was subjected to a shorter period of weathering.

The progressive amplification of hot and humid climatic conditions was continued before the deposition of silty sand horizon DS-4. This horizon is the result of several high-energy floods under amplified humid climatic events. Very low chemical weathering, inadequate pedogenic features and distinct depositional structures (i.e., ripple stratification, Fig. 9) designate the depositional period of DS-4 as well as amplified humid climatic events was relatively short. In addition, the erosional surface between the paleosol DGS-4 and sediment unit DS-4 indicates the period of non-deposition and subsequently the abrupt climatic change from drier to humid phases.

4.8.2.2. Climatic cycle II. After the completion of the climatic cycle *I*, the climate turns to semi-arid to sub-humid conditions. At the beginning of this cycle, sedimentation took place under low-energy floods with the formation of very weakly developed paleosol DGS-3 (Figs. 2 and 9) as revealed from the sediment and pedogenic characteristics. Very low thickness with little pedogenic signatures of this paleosol indicates the extent of the climatic event prevailed for a very short period. At the end of semi-arid to sub-humid events, climate again shifted to humid conditions which is consistent with the ripple laminated sandy deposits of DS-3 that deposited under high energy conditions. It seems to be the development period of paleosol DGS-3 and silty sand horizon of DS-3, represents the duration of climatic cycle *II* is significantly shorter than other climatic cycles as discussed in this section.

4.8.2.3. Climatic cycles III. At the beginning of the cycle *III*, low energy sedimentation along with pedogenic processes operated to form the weakly developed Inceptisol-like paleosol DGS-2 (Figs. 2 and 9). Based on relatively higher values of geochemical proxies (CIA, CIW, and CIA-K) and abundances of pedogenic-biogenic features, DGS-2 is considered as relatively more weathered and also denotes the longer development period in comparison to other paleosols found in gray unit/NA unit. Applying geochemical climofunction (Sheldon, 2006c), the estimated MAT is found as 28.3 ± 0.6 °C (Fig. 9 and Table 3) which is 2 °C higher than the present MAT of the area. However, non-deposition or very slow rate of sedimentation (based on paleosol thickness) and relatively low TOC% concentration are possibly the results of hydrological drought as well as low precipitation. It is important to note that historical climatic records indicate that both the Indian region and our study area experienced extreme temperatures with reduced precipitation during several historical periods. For instance, South Asia has faced episodes of extreme heat alongside significant drought conditions. This discrepancy between high temperatures and low precipitation reflects such historical climatic extremes. The upper part of the cycle is characterized by ripple laminated thick silty sand unit (DS-2) with negligible post-depositional alteration that represents sedimentation processes under relatively hot and humid climate. Therefore, it indicates that climatic cycle III started with comparatively hot and arid to sub-humid and finally completed with abrupt shifting towards extremely warm and humid climatic conditions.

A similar climatic phase is also recognized in adjoining areas and many other parts of the globe especially in the Indian regions and this period may correspond to the Medieval Warming Period (MWP). Phytolith analysis of archaeological soils in Somapura Mahavihara, Paharpur, very close to our study area pointed out that warmer climates persisted from around 850 CE–915 (Alam et al., 2009). Rühland et al. (2006) carried out a palynological study of a peat bog in the Higher Central Himalaya and indicated a wetter period of around 700 years BP and another similar study of the Naychhudwari bog (Himachal Pradesh) has discovered a warm/moist phase from 1300yr to 750 yr BP (Chauhan, 2006). The Juniper chronologies from western high Asia (Karakoram, Tien Shan) also point to a warm period from 1000 yrs. BP to 750 yr. BP (Esper et al., 2007). An extended period of warmth has also been reported BP and 550 yr BP is further confirmed by stable carbon isotope analysis on the sub-Alpine Juniper from eastern Tibet (Zimmermann et al., 1997; Helle et al., 2002). A radiocarbon-dated in the Sargasso Sea (North Atlantic) shows that the sea surface temperature during the Medieval Warm Period (MWP) was approximately 1 °C warmer than today. From the evolution of global temperature at MWP, it is realized that the estimated very hot temperature (MAT: 28.3 ± 0.6 °C) is more consistent with the Medieval Warming Period (~ 920-440 yr BP).

4.8.2.4. Climatic cycle IV. At the end of the Medieval Warm Period (MWP), climate was again shifted toward cool and drier conditions called the Little Ice Age (LIA) when the global average temperature was probably about 0.5 °C cooler than that started at the beginning of the 20th century (Warrick and Ahmed, 1996). The LIA began somewhere between the 13th and 16th centuries and finished in the mid-19th century AD. It is documented from 1600 CE–1950 in the western Himalayan tree ring records (Yadav and Singh, 2002) and from 1605 CE–1770 in Nepal (Cook et al., 2003). The effects of this climatic event are best documented in Europe though there is evidence that it was a global phenomenon (Grove, 1988). The historical records on the frequency of droughts, dust storms, and floods in China also show that the climate was highly uneven during the LIA (Zhang and Crowley, 1989).

The signature of LIA can also be recognized in climatic cycle IV of the present study. The very hot temperature and humid events of climatic cycle III gradually shifted to relatively cooler and arid since climatic cycle IV started. Geochemical data of the present study indicate that the development processes of weakly developed Inceptisol-like paleosol of DGS-1 of this cycle were influenced by LIA global climatic events. The estimated MAT for paleosol DGS-1 is 24 ± 0.6 °C (Sheldon, 2006c) (Fig. 9 and Table 3) which is an average 2 °C cooler than the present MAT conditions. The other geochemical indices also suggest a relatively cooler climate during the development of paleosol DGS-1. The geochemical data support a relatively cooler and sub-humid to humid

climate during the development of this paleosol, consistent with the low energy sedimentation and limited pedogenic features observed. These conditions are typical of weakly developed paleosols under low temperature and low precipitation regimes, unlike the more robust profiles in warmer, wetter climates throughout the development periods of paleosol DGS-1.

This climatic cycle also terminated with a gradual shift from cooler, arid to warmer, humid climatic events. Therefore, increased rainfall might have been rise to high-energy floods, and finally ripple laminated silty sand unit DS-1 that was deposited on the surface of paleosol DGS-1. Low chemical weathering and insignificant pedogenic signature in this unit also represent rapid as well as shorter periods of deposition.

4.8.2.5. Climatic cycle V. At the beginning of climatic cycle *V*, higher precipitation rates of cycle IV gradually declined. Therefore, depositional floodplains experienced low-energy floods which received finer sediments. These finer sediments converted to Inceptisol like modern soil DMS (Figs. 2 and 9) due to pedogenic activities. The moderately defined Bw horizon and surface position of this soil indicate that these are the most recent deposits and formed under present-day climatic conditions. Applying the geochemical climofunctions (Sheldon, 2006c), the estimated MAT is found to be 26.1 ± 0.6^0C (Fig. 9 and Table 3) which is more consistent with today's hot and humid climatic conditions.

The extreme events of aridity and humid conditions are most probably the results of ENSO (El Niño: Southern Oscillations) effects. The geographical features and location of Bangladesh indicate that this area is particularly susceptible to the effects of ENSO during the late Holocene. During El Niño events the sea-level pressure gradients in the southeastern Pacific weaken, accompanied by a decrease in the strength of trade winds, resulting in reductions to rainfall in Bangladesh during El Niño years while La Niña years are associated with increased rainfall and floods (Ahmed, 1993; Choudhury, 1994; Shaman and Tziperman, 2005; Belliard et al., 2021). Choudhury (1994) has pointed out, that extensive famines in Bangladesh in the historical period are strongly correlated with El Niño events (e.g. 1770, 1943, 1974, and 1982 famines), typically as a result of reduced rainfall causing crops to fail, with the situation exacerbated by severe flooding associated with the transition into La Niña years. Such events cause massive reductions in agricultural productivity and production, leading to widespread poverty, migration, and social unrest. The buried past settlements in the area were most probably demised due to the effects of the El Niño phenomenon with the highest aridity.

Finally, the past climatic reconstruction is a very difficult process because so many parameters are needed to ensure precise estimations. Although the present study represents very well correlations between paleosol development and climatic interactions. The present study revealed that there were several climatic fluctuations (episodes with events) occurred in the study area during the Quaternary periods which are consistent with climatic fluctuations recognized in the neighboring regions and several parts of the world.

4.9. Limitations for this study

The present study has some limitations. We acknowledge the importance of obtaining more precise age control of the sediments succession in the study. Despite these limitations, the study has provided valuable insights into the Quaternary environment and climate change reconstruction. The findings offer significant contributions to our understanding of the Quaternary environment and climatic conditions of NW Bangladesh.

5. Conclusions

Quantitative estimation of the Quaternary continental paleoclimatic (MAP and MAT) record is rare in Bangladesh. In this paper, we study different paleosols at two vertical lithological sections i.e., Durgadaha (DD) and Kujishahar (KS) sections in east-central Barind, NW Bangladesh to reconstruct the paleoclimate (MAP and MAT) and paleoenvironment of the area. The Quaternary deposits of the studied area have been broadly classified into two categories i) Gray unit/Newer Alluvium (NA) unit at the upper part and ii) Red unit/Older Alluvium (OA) unit at the bottom. Both units contain many paleosols. The red unit paleosols are considered as of Early Pleistocene and the Gray unit of Late Holocene with a maximum age of ~1300yr. BP (Archaeological dating). Both field observation, major and trace element geochemical evidence indicates the red unit paleosols are moderate to intensely weathered and pedogenically altered and marked as moderate to strongly developed (i.e., equivalent to Oxisols, Ultisol, and Aridisol). However, gray unit paleosols were developed in recent alluvial deposits, marked as moderate to weakly developed (Inceptisol and Entisol). Field observation and geochemical characteristics represent two significant long-term climatic episodes in the Early Pleistocene and five short-term climatic cycles during the late Holocene since 1300yr BP. Estimated paleo MAP (i.e., 1000 ± 181 mm) and MAT (i.e., 9° ± 4.4 °C) significantly represent that the lower part of Early Pleistocene (DGS-6/KGS-4) was arid to semi-arid. The middle part of the Early Pleistocene (DGS-5/KGS-3) was semiarid to sub-humid as reflected by the estimated MAP and MAT. Five short-term climatic cycles are very significantly observed in the late Holocene during the last 1300 years. Those cycles are remarkable from each other and every single cycle started with a relatively drier (set of droughts) event and ended with a more humid (set of floods) event. At about 1300yr. BP (i.e., archaeological period), climatic cycle-I was started (DGS-4) with relatively cool, arid/dry (MAT: 23.1° ± 0.6 °C) climate that largely affected the demise of paleo-settlement and later one this climate turned towards humid event (DS-4) with high energy floods. Similarly, climatic cycle-II started and ended with relatively dry and humid (DGS-3 and DS-3) conditions respectively. Climatic cycle-III is more significant due to its very hot (MAT: 28.3° ± 0.6 °C) climatic condition which seems to be more consistent with the Medieval Warm Period (MWP) of global climatic events. This cycle also began with hot and dry (DGS-2) conditions and completed with extreme humid (DS-2) phases. Climatic cycle-IV is also similar in nature (DGS-1 and DS-1) but significant for relatively cooler/drier conditions (MAT: 24° ± 0.6 °C) and can be compared with Little Ice Age (LIA) events of global climates. Climatic cycle-V is still ongoing (DMS) and the estimated MAT is 26.1 ± 0.6 °C which is found to be more consistent with the present MAT trend of the area.

CRediT authorship contribution statement

Md. Sha Alam: Writing – review & editing, Writing – original draft, Investigation, Data curation, Conceptualization. **Md. Shafiqul Alam:** Writing – review & editing, Writing – original draft, Investigation, Conceptualization. **Mohammad Nazim Zaman:** Writing – review & editing, Writing – original draft. **Ayon Saha:** Writing – review & editing, Writing – original draft. **Md Mahmudul Hasan Rakib:** Writing – review & editing, Writing – original draft. **Arabe Khan:** Writing – original draft, Writing – review & editing. **Rahat Khan:** Writing – original draft, Writing – review & editing. **Dhiman Kumer Roy:** Writing – review & editing, Writing – original draft, Conceptualization.

Declaration of competing interest

The authors declare that they have no known competing financial interests or personal relationships that could have appeared to influence the work reported in this paper.

Data availability

Data will be made available on request.

Acknowledgements

The authors would like to express their thanks to the authority of the Institute of Mining, Mineralogy and Metallurgy (IMMM), Joypurhat, Bangladesh for providing facilities for geochemical analysis. Constructive reviews by Prof. Daham and anonymous reviewer significantly improved the manuscript, and were much appreciated. The authors express their gratitude to the editor Ana B. Marín-Arroyo for valuable comments and suggestions which improved the quality of the manuscript.

References

Achyuthan, H., Thirunavukarasu, N., 2009. Quaternary stratigraphy of the Koratallaiyar-Cooum basin, Chennai. J. Geol. Soc. India 73, 683–696. https://doi.org/10.1007/s12594-009-0053-5.

Ahmed, A., 1993. A climatological study of Bangladesh and possible correlation with El Niño/Southern Oscillation. Unpublished Master of Science Dissertation, University of Dhaka, Bangladesh.

Alam, M.S., 1993. Stratigraphical and paleo-climatic studies of the quaternary deposits in north-western Bangladesh. Unpublished D. Sc. Thesis Submitted to Vrije University, Brussels, Belgium.

Alam, A.K.M.K., Khan, M.S.H., 2022. Geomorphology of Bangladesh and potential land use. Bangladesh Geosciences and Resources Potential. CRC Press, pp. 355–398.

Alam, M.S., Paepe, R., 1996. Palaeosols in the Quaternary stratigraphy in north-western Bangladesh. Bangladesh Journal of Geology 2, 15–36.

Alam, Shafiqul, M., Keppens, E., Paepe, R., 1997. The use of oxygen and carbon isotope composition of pedogenic carbonates from Pleistocene palaeosols in NW Bangladesh, as palaeoclimatic indicators. Quat. Sci. Rev. 16 (2), 161–168. https://doi.org/10.1016/S0277-3791(96)00044-3.

Alam, A.K.M.M., Xie, S., Saha, D.K., Chowdhury, S.Q., 2008. Clay mineralogy of archaeological soil: an approach to paleoclimatic and environmental reconstruction of the archaeological sites of the Paharpur area, Badalgacchi upazila, Naogaon district. Bangladesh. Environmental Geology 53 (8), 1639–1650. https://doi.org/10.1007/s00254-007-0771-1.

Alam, A.K.M.M., Xie, S., Wallis, L.A., 2009. Reconstructing late Holocene palaeoenvironments in Bangladesh: phytolith analysis of archaeological soils from Somapura Mahavihara site in the Paharpur area, badalgacchi upazila, naogaon district, Bangladesh. J. Archaeol. Sci. 36 (2), 504–512. https://doi.org/10.1016/j.jas.2008.09.038.

Almogi-Labin, A., 2011. The paleoclimate of the Eastern Mediterranean during the transition from early to mid Pleistocene (900 to 700 ka) based on marine and non-marine records: an integrated overview. J. Hum. Evol. 60 (4), 428–436. https://doi.org/10.1016/j.jhevol.2010.03.007.

Amorosi, A., Bruno, L., Campo, B., Di Martino, A., Sammartino, I., 2021. Patterns of geochemical variability across weakly developed paleosol profiles and their role as regional stratigraphic markers (Upper Pleistocene, Po Plain). Palaeogeogr. Palaeoclimatol. Palaeoecol. 574, 110413 https://doi.org/10.1016/j.palaeo.2021.110413.

Aquino, A., Scardia, G., Prud'homme, C., Dave, A.K., Lezzerini, M., Johansson, A.E., Marquer, L., Safaraliev, N., Lauer, T., Fitzsimmons, K.E., 2024. Variability in geochemical weathering indices in loess over the last full glacial cycle at Karamaidan, central Asia (Tajikistan). Front. Earth Sci. 12, 1347910 https://doi.org/10.3389/feart.2024.1347910.

Babeesh, C., Achyuthan, H., Jaiswal, M.K., Lone, A., 2017. Late Quaternary loess-like paleosols and pedocomplexes, geochemistry, provenance and source area weathering, Manasbal, Kashmir Valley, India. Geomorphology 284, 191–205. https://doi.org/10.1016/j.geomorph.2017.01.004.

Baillie, I.C., 2001. Soil Survey Staff 1999, soil taxonomy. Soil Use Manag. 17 (1), 57–60. https://doi.org/10.1111/j.1475-2743.2001.tb00008.x.

Belliard, J.-P., Dominguez-Granda, L.E., Ramos-Veliz, J.A., Rosado-Moncayo, A.M., Nath, J., Govers, G., Gourgue, O., Temmerman, S., 2021. El Niño driven extreme sea levels in an Eastern Pacific tropical river delta: landward amplification and shift from oceanic to fluvial forcing. Global Planet. Change 203, 103529. https://doi.org/10.1016/j.gloplacha.2021.103529.

Beverly, E.J., Lukens, W.E., Stinchcomb, G.E., 2018. Paleopedology as a tool for reconstructing paleoenvironments and paleoecology. Methods in Paleoecology: Reconstructing Cenozoic Terrestrial Environments and Ecological Communities 151–183. https://doi.org/10.1007/978-3-319-94265-0_9.

Birkeland, P.W., 1984. Soils and Geomorphology.

Caran, S.C., 1998. Quaternary paleoenvironmental and paleoclimatic reconstruction: a discussion and critique, with examples from the southern High Plains. Plains Anthropol. 43 (164), 111–124. https://doi.org/10.1080/2052546.1998.11931894.

Carey, C., Howard, A.J., Jackson, R., Brown, A., 2017. Using geoarchaeological deposit modelling as a framework for archaeological evaluation and mitigation in alluvial environments. J. Archaeol. Sci.: Report 11, 658–673. https://doi.org/10.1016/j.jasrep.2017.01.013.

Certini, G., Scalenghe, R., 2023. The crucial interactions between climate and soil. Sci. Total Environ. 856, 159169 https://doi.org/10.1016/j.scitotenv.2022.159169.

Chauhan, M.S., 2006. Late Holocene vegetation and climate change in the alpine belt of Himachal Pradesh. Curr. Sci. 1562–1567.

Chauhan, M.S., Sharma, C., 2000. Late Holocene vegetation and climate in dewar tal area, inner lesser garhwal Himalaya. Journal of Palaeosciences 49, 1–3. https://doi.org/10.54991/jop.2000.164, 509–514.

Chen, L., Lai, X., Zhao, Y., Chen, H., Ni, Z., 2011. Organic carbon isotope records of paleoclimatic evolution since the last glacial period in the Tangjia region, Tibet. J. Earth Sci. 22, 704–717. https://doi.org/10.1007/s12583-011-0221-6.

Chen, H.-F., Yeh, P.-Y., Song, S.-R., Hsu, S.-C., Yang, T.-N., Wang, Y., Chi, Z., Lee, T.-Q., Chen, M.-T., Cheng, C.-L., 2013. The Ti/Al molar ratio as a new proxy for tracing sediment transportation processes and its application in aeolian events and sea level change in East Asia. J. Asian Earth Sci. 73, 31–38. https://doi.org/10.1016/j.jseaes.2013.04.017.

Choudhury, A.M., 1994. International centre for theoretical physics. Bangladesh floods, cyclones and ENSO.

Cook, E.R., Krusic, P.J., Jones, P.D., 2003. Dendroclimatic signals in long tree-ring chronologies from the Himalayas of Nepal. Int. J. Climatol.: A Journal of the Royal Meteorological Society 23 (7), 707–732. https://doi.org/10.1002/joc.911.

da Silva Neto, E.C., Pereira, M.G., dos Anjos, L.H.C., Calegari, M.R., Azevedo, A.C., Schiavo, J.A., Pessenda, L.C.R., 2020. Phytoliths as paleopedological records of an histosol-cambisol-ferralsol sequence in Southeastern Brazil. Catena 193, 104642. https://doi.org/10.1016/j.catena.2020.104642.

Delgado, L., Batezelli, A., Ladeira, F.S.B., 2021. Paleoenvironmental and paleoclimatic reconstruction of Lower to Upper Cretaceous sequences of the Bauru Basin based on paleosol geochemistry and mineralogical analyses. Palaeogeogr. Palaeoclimatol. Palaeoecol. 569, 110328 https://doi.org/10.1016/j.palaeo.2021.110328.

El-Asmar, H.M., 2023. Quaternary environmental and climatic changes in Egypt: proxies from sedimentary records. The Phanerozoic Geology and Natural Resources of Egypt 425–489. https://doi.org/10.1007/978-3-030-95637-0_16.

Esper, J., Frank, D., Büntgen, U., Verstege, A., Luterbacher, J., Xoplaki, E., 2007. Long-term drought severity variations in Morocco. Geophys. Res. Lett. 34 (17), 1–5. https://doi.org/10.1029/2007GL030844.

Eze, P.N., Molwalefhe, L.N., Kebonye, N.M., 2021. Geochemistry of soils of a deep pedon in the Okavango Delta, NW Botswana: implications for pedogenesis in semi-arid regions. Geoderma Regional 24, e00352.

Fedo, C.M., Wayne Nesbitt, H., Young, G.M., 1995. Unraveling the effects of potassium metasomatism in sedimentary rocks and paleosols, with implications for paleoweathering conditions and provenance. Geology 23 (10), 921–924. https://doi.org/10.1130/0091-7613(1995)023.3C0921:UTEOPM.3E2.3.CO;2.

Froese, D.G., Barendregt, R.W., Enkin, R.J., Baker, J., 2000. Paleomagnetic evidence for multiple late pliocene-early Pleistocene glaciations in the klondike area, yukon territory. Can. J. Earth Sci. 37 (6), 863–877. https://doi.org/10.1139/e00-014.

Ghasera, K.M., Rashid, S.A., 2024. Influence of micro-scale factors in weathering and elements mobility: evidence from a comparative study of granite and basalt weathering profiles across India. Catena 235, 107680. https://doi.org/10.1016/j.catena.2023.107680.

Gillot, T., Cojan, I., Badia, D., 2022. Paleoclimate instabilities during late Oligocene-Early Miocene in SW Europe from new geochemical climofunctions based on soils with pedogenic carbonate. Palaeogeogr. Palaeoclimatol. Palaeoecol. 591, 110882 https://doi.org/10.1016/j.palaeo.2022.110882.

Goiran, J.-P., Chan, W.M., Benech, C., Vitale, Q.V., Riddick, N., Delile, H., Salomon, F., Chapkanski, S., Oberlin, C., Brocard, G.Y., 2022. Developments in geoarchaeological research, methodologies and applications in harbour maritime Archaeology. Seasides of Byzantium: Harbours and Anchorages of a Mediterranean Empire 21, 109–129.

Gong, Z., Zhang, M., Li, J., Huang, C., 2023. Late Permiañ 6 My cooling induced by basaltic weathering of the Emeishan large igneous province: evidence from interbasaltic paleosols. Palaeogeogr. Palaeoclimatol. Palaeoecol. 609, 111305 https://doi.org/10.1016/j.palaeo.2022.111305.

Goñi, M.F.S., 2022. The climatic and environmental context of the Late Pleistocene. Updating Neanderthals. Elsevier, pp. 17–38. https://doi.org/10.1016/B978-0-12-821428-2.00017-2.

Grimaud, J.-L., Grall, C., Goodbred, S., Steckler, M.S., Sincavage, R., Pickering, J.L., Paola, C., Seeber, L., Hossain, M.S., 2020. Flexural deformation controls on late quaternary sediment dispersal in the garo-rajmahal gap, NW Bengal Basin. Basin Res. 32 (5), 1242–1260. https://doi.org/10.1111/bre.12425.

Groot, J.J., 1991. Palynological evidence for late Miocene, Pliocene and early Pleistocene climate changes in the middle US Atlantic coastal plain. Quat. Sci. Rev. 10 (2–3), 147–162. https://doi.org/10.1016/0277-3791(91)90015-M.

Grove, J.M., 1988. The Little Ice Age Methuen London. UK.

Guo, X., Retallack, G.J., He, L., Li, Z., Liu, J., Wang, R., Liu, X., Wang, W., 2024. Northwestern Chinese record of Cenozoic global events. Catena 239, 107892. https://doi.org/10.1016/j.catena.2024.107892.

Haque, M.M., Hoyanagi, K., 2021. Influences of sea level on depositional environment during the last 1000 years in the southwestern Bengal delta. Bangladesh. The Holocene 31 (6), 915–925. https://doi.org/10.1177/0959683621994671.

Harnois, L., 1988. The CIW index: a new chemical index of weathering. Sediment. Geol. 55 (3–4), 319–322. https://doi.org/10.1016/0037-0738(88)90137-6.

Haug, G.H., Gunther, D., Peterson, L.C., Sigman, D.M., Hughen, K.A., Aeschlimann, B., 2003. Climate and the collapse of Maya civilization. Science 299 (5613), 1731–1735. https://doi.org/10.1126/science.1080444.

Heine, K., Völkel, J., 2010. Soil clay minerals in Namibia and their significance for the terrestrial and marine past global change research. Afr. study Monogr. Suppl. issue 40, 31–50. https://doi.org/10.14989/96299.

Helle, G., Schleser, G.H., Bräuning, A., 2002. Climate History of the Tibetan Plateau for the Last 1500 Years as Inferred from Stable Carbon Isotopes in Three-Rings.

Hou, K., Zhang, Y., Qian, H., Zhang, Q., Qu, W., Ren, W., 2022. Insight into the environmental significance of grain-size fractal and pedogenesis of a typical loess

and paleosol sequence. Catena 215, 106337. https://doi.org/10.1016/j.catena.2022.106337.
Hughes, Philip D., Gibbard, P.L., 2018. Global glacier dynamics during 100 ka Pleistocene glacial cycles. Quaternary Research 90 (1), 222–243. https://doi.org/10.1017/qua.2018.37.
Hughes, P.D., Woodward, Jc, Gibbard, P.L., 2006. Late Pleistocene glaciers and climate in the mediterranean. Global Planet. Change 50 (1–2), 83–98. https://doi.org/10.1016/j.gloplacha.2005.07.005.
Huot, H., Simonnot, M.-O., Morel, J.L., 2015. Pedogenetic trends in soils formed in technogenic parent materials. Soil Sci. 180 (4), 182–192. https://doi.org/10.1097/SS.0000000000000135.
Hussain, S., Sharma, V., Arya, V.M., Sharma, K.R., Rao, C.S., 2019. Total organic and inorganic carbon in soils under different land use/land cover systems in the foothill Himalayas. Catena 182, 104104. https://doi.org/10.1016/j.catena.2019.104104.
Khan, F.H., 1991. Geology of Bangladesh. Wiley Eastern.
Khan, A.A., Rahman, T., 1992. An analysis of the gravity field and tectonic evaluation of the northwestern part of Bangladesh. Tectonophysics 206 (3–4), 351–364. https://doi.org/10.1016/0040-1951(92)90386-K.
Khandoker, R.A., 1987. Origin of elevated Barind-Madhupur areas, Bengal basin: result of neotectonic activities. Bangladesh Journal of Geology 6 (2), 1–9.
Kogler, S.J., Hembree, D.I., 2019. Influences of modern pedogenesis on paleoclimate estimates from pennsylvanian and permian paleosols, southeast Ohio, USA. J. Sediment. Res. 89 (3), 227–241. https://doi.org/10.2110/jsr.2019.11.
Kotlia, B.S., Joshi, L.M., 2013. Late Holocene climatic changes in garhwal Himalaya. Curr. Sci. 911–919.
Kraus, M.J., 1999. Paleosols in clastic sedimentary rocks: their geologic applications. Earth Sci. Rev. 47 (1–2), 41–70. https://doi.org/10.1016/S0012-8252(99)00026-4.
Kuehl, S.A., Allison, M.A., Goodbred, S.L., Kudrass, H., 2005. The Ganges-Brahmaputra Delta.
Kumar, A., Ray, Y., Ghosh, R., Bandyopadhyay, S., Singh, V., Srivastava, P., 2020. Late Quaternary sedimentation history of the Himalaya and its foreland. Episodes Journal of International Geoscience 43 (1), 498–510. https://doi.org/10.18814/epiiugs/2020/020032.
Kumaravel, V., Sangode, S.J., Siva Siddaiah, N., Kumar, R., 2009. Major element geochemical variations in a Miocene-Pliocene Siwalik paleosol sequence: implications to soil forming processes in the Himalayan Foreland Basin. J. Geol. Soc. India 73, 759–772. https://doi.org/10.1007/s12594-009-0061-5.
Kurtz, A.C., Derry, L.A., Chadwick, O.A., Alfano, M.J., 2000. Refractory element mobility in volcanic soils. Geology 28 (8), 683–686.
Li, T.L., 2000. A Compendium of Geochemistry—The Elemental Composition Changes from Solar Nebula to the Human Brain. Princeton Univ. Press.
Li, J., Li, F., Liu, Q., Zhang, Y., 2014. Trace metal in surface water and groundwater and its transfer in a Yellow River alluvial fan: evidence from isotopes and hydrochemistry. Sci. Total Environ. 472, 979–988. https://doi.org/10.1016/j.scitotenv.2013.11.120.
Liivamägi, S., Środoń, J., Bojanowski, M.J., Stanek, J.J., Roberts, N.M.W., 2021. Precambrian paleosols on the great unconformity of the east European craton: an 800 million year record of baltica's climatic conditions. Precambrian Res. 363, 106327 https://doi.org/10.1016/j.precamres.2021.106327.
Mahmoud, Ben, K, R., Zurqani, H.A., 2021. Soil forming factors and processes. The Soils of Libya 33–48. https://doi.org/10.1007/978-3-030-66368-1_3.
Matchavariani, L., 2019. Soil-forming factors. The Soils of Georgia 19–50. https://doi.org/10.1007/978-3-030-18509-1_3.
Matshameko, Y., Kebonye, N.M., Eze, P.N., 2022. Ethnopedological knowledge and scientific assessment of earthenware pottery-making soils of southern Botswana for natural resource management. Geoderma Regional 31, e00580. https://doi.org/10.1016/j.geodrs.2022.e00580.
Maynard, J.B., 1992. Chemistry of modern soils as a guide to interpreting Precambrian paleosols. J. Geol. 100 (3), 279–289.
Mazari, R.K., Bagati, T.N., Chauhan, M.S., Rajagopalan, G., 1995. Palaeoclimatic record of last 2000 years in trans-Himalayan Lahaul-Spiti region. Paleoclimate and Environmental Variability in Austral-Asian Transect during the Past 2000 Years 262–269.
McLennan, S.M., Hemming, S., McDaniel, D.K., Hanson, G.N., 1993. Geochemical approaches to sedimentation, provenance, and tectonics. Spec. Pap. Geol. Soc. Am. 284, 21–40. https://doi.org/10.1130/SPE284-p21.
Mei, H., Jian, X., Zhang, W., Fu, H., Zhang, S., 2021. Behavioral differences between weathering and pedogenesis in a subtropical humid granitic terrain: implications for chemical weathering intensity evaluation. Catena 203, 105368. https://doi.org/10.1016/j.catena.2021.105368.
Meyers, P.A., Lallier-Vergès, E., 1999. Lacustrine sedimentary organic matter records of Late Quaternary paleoclimates. J. Paleolimnol. 21 (3), 345–372. https://doi.org/10.1023/A:1008073732192.
Mikkonen, H.G., Dasika, R., Drake, J.A., Wallis, C.J., Clarke, B.O., Reichman, S.M., 2018. Evaluation of environmental and anthropogenic influences on ambient background metal and metalloid concentrations in soil. Sci. Total Environ. 624, 599–610. https://doi.org/10.1016/j.scitotenv.2017.12.131.
Monsur, M.H., 1995. Textural characteristics of the quaternery deposits of the Barind area of the Bengal Basin. Bangladesh. Bangladesh J. Sci. Res 13 (2), 111–117.
Monsur, Hussain, M, D., Paepe, R., 1992. Quaternary stratigraphy of the Barind area of the Bengal basin. Bangladesh. Indian Journal of Earth Sciences 19 (2–3), 79–84.
Morgan, J.P., McIntire, W.G., 1959. Quaternary geology of the Bengal basin, east Pakistan and India. Geol. Soc. Am. Bull. 70 (3), 319–342. https://doi.org/10.1130/0016-7606(1959)70[319:QGOTBB]2.0.CO;2.
Morrill, C., Overpeck, J.T., Cole, J.E., 2003. A synthesis of abrupt changes in the Asian summer monsoon since the last deglaciation. Holocene 13 (4), 465–476. https://doi.org/10.1191/0959683603hl639ft.
Moussavi-Harami, R., Mahboubi, A., Nadjafi, M., Brenner, R.L., Mortazavi, M., 2009. Mechanism of calcrete formation in the Lower Cretaceous (Neocomian) fluvial deposits, northeastern Iran based on petrographic, geochemical data. Cretac. Res. 30 (5), 1146–1156. https://doi.org/10.1016/j.cretres.2009.04.003.
Muhs, D.R., 2021. Soils and Paleosols.
Mukherjee, A., Fryar, A.E., Thomas, W.A., 2009. Geologic, geomorphic and hydrologic framework and evolution of the Bengal basin, India and Bangladesh. J. Asian Earth Sci. 34 (3), 227–244. https://doi.org/10.1016/j.jseaes.2008.05.011.
Munsell, A.H., 1975. Munsell soil color charts. Munsell color.
Naiman, R.J., Bechtold, J.S., Drake, D.C., Latterell, J.J., O'Keefe, T.C., Balian, E.V., 2005. Origins, patterns, and importance of heterogeneity in riparian systems. Ecosystem Function in Heterogeneous Landscapes 279–309. https://doi.org/10.1007/0-387-24091-8_14.
Nandy, J., Nath, V., 2021. Sedimentology of tertiary and quaternary gravel and sand beds of dhalbhumgarh-chakuliya-baharagora area, east singhbhum district, India. Int. J. Res. Appl. Sci. Eng. Technol. 9 (4), 70–93.
Nash, D.J., 2022. Calcretes, silcretes and intergrade duricrusts. Landscapes and Landforms of Botswana. Springer, pp. 223–246. https://doi.org/10.1007/978-3-030-86102-5_13.
Neidhardt, H., Biswas, A., Freikowski, D., Majumder, S., Chatterjee, D., Berner, Z.A., 2013. Reconstructing the sedimentation history of the Bengal Delta Plain by means of geochemical and stable isotopic data. Appl. Geochem. 36, 70–82. https://doi.org/10.1016/j.apgeochem.2013.06.017.
Nelson, D.W., Sommers, L.E., 1983. Total carbon, organic carbon, and organic matter. Methods of Soil Analysis: Part 2 Chemical and Microbiological Properties 9, 539–579.
Nesbitt, Hw, Young, G.M., 1982. Early Proterozoic climates and plate motions inferred from major element chemistry of lutites. Nature 299 (5885), 715–717. https://doi.org/10.1038/299715a0.
Nesbitt, H.W., Young, G.M., 1984. Prediction of some weathering trends of plutonic and volcanic rocks based on thermodynamic and kinetic considerations. Geochem. Cosmochim. Acta 48 (7), 1523–1534. https://doi.org/10.1016/0016-7037(84)90408-3.
Nesbitt, H.W., Young, G.M., 1989. Formation and diagenesis of weathering profiles. J. Geol. 97 (2), 129–147.
Nordt, L.C., Driese, S.G., 2010. A modern soil characterization approach to reconstructing physical and chemical properties of paleo-Vertisols. Am. J. Sci. 310 (1), 37–64. https://doi.org/10.2475/01.2010.02.
Perri, F., 2020. Chemical weathering of crystalline rocks in contrasting climatic conditions using geochemical proxies: an overview. Palaeogeogr. Palaeoclimatol. Palaeoecol. 556, 109873 https://doi.org/10.1016/j.palaeo.2020.109873.
Prochnow, S.J., Nordt, L.C., Atchley, S.C., Hudec, M.R., 2006. Multi-proxy paleosol evidence for middle and late Triassic climate trends in eastern Utah. Palaeogeogr. Palaeoclimatol. Palaeoecol. 232 (1), 53–72. https://doi.org/10.1016/j.palaeo.2005.08.011.
Profe, J., Neumann, L., Novothny, Á., Barta, G., Rolf, C., Frechen, M., Ohlendorf, C., Zolitschka, B., 2018. Paleoenvironmental conditions and sedimentation dynamics in Central Europe inferred from geochemical data of the loess-paleosol sequence at Süttő (Hungary). Quat. Sci. Rev. 196, 21–37. https://doi.org/10.1016/j.quascirev.2018.07.034.
Pye, K., Krinsley, D.H., 1986. Diagenetic carbonate and evaporite minerals in Rotliegend aeolian sandstones of the southern North Sea: their nature and relationship to secondary porosity development. Clay Miner. 21 (4), 443–457. https://doi.org/10.1180/claymin.1986.021.4.03.
Raigemborn, M.S., Lizzoli, S., Hyland, E., Cotton, J., Peral, L.E.G., Beilinson, E., Krause, J.M., 2022. A paleopedological approach to understanding Eocene environmental conditions in southern Patagonia, Argentina. Palaeogeogr. Palaeoclimatol. Palaeoecol. 601, 111129.
Raigemborn, M.S., Lizzoli, S., Moyano-Paz, D., Varela, A.N., Poiré, D.G., Loinaze, V.P., Vera, E., Manabe, M., Novas, F., 2023. Paleosols of the maastrichtian dinosaur-bearing chorrillo formation (southern patagonia, Argentina): paleoenvironmental and paleoclimate implications. Cretac. Res. 150, 105587 https://doi.org/10.1016/j.cretres.2023.105587.
Rashid, B., Islam, B., 2018. Structure and Lineaments of the Northwestern Part of Bangladesh and Evolution of the Barind Tract. 5 (3), 26–36.
Rashid, B., Islam, S.U., Islam, B., 2015. River morphology and evolution of the Barind tract, Bangladesh. J. Nepal Geol. Soc. 49 (1), 65–76. https://doi.org/10.3126/jngs.v49i1.23144.
Retallack, G.J., 1995. Palaeosols of the siwalik group as a 15 Mys record of South Asian palaeoclimate. Mem. Geol. Soc. India 32, 36–51.
Retallack, G.J., 2001. Cenozoic expansion of grasslands and climatic cooling. J. Geol. 109 (4), 407–426.
Retallack, Gregory J., 2004. Late Oligocene bunch grassland and early Miocene sod grassland paleosols from central Oregon, USA. Palaeogeogr. Palaeoclimatol. Palaeoecol. 207 (3–4), 203–237. https://doi.org/10.1016/j.palaeo.2003.09.027.
Retallack, Gregory J., 2008. Soils of the Past: an Introduction to Paleopedology. John Wiley and Sons.
Retallack, Gregory J., 2016. Field and laboratory tests for recognition of Ediacaran paleosols. Gondwana Res. 36, 107–123. https://doi.org/10.1016/j.gr.2016.05.001.
Rieu, R., Allen, P.A., Plötze, M., Pettke, T., 2007. Climatic cycles during a Neoproterozoic "snowball" glacial epoch. Geology 35 (4), 299–302. https://doi.org/10.1130/G23400A.1.

Ripley, J.L., 1998. A geoarchaeological approach to using surface sites for paleoenvironmental reconstructions. Geoarchaeology: Int. J. 13 (8), 793–818.
Rodrigo-Gámiz, M., Martínez-Ruiz, F., Chiaradia, M., Jiménez-Espejo, F.J., Ariztegui, D., 2015. Radiogenic isotopes for deciphering terrigenous input provenance in the western Mediterranean. Chem. Geol. 410, 237–250. https://doi.org/10.1016/j.chemgeo.2015.06.004.
Rohling, E.J., Yu, J., Heslop, D., Foster, G.L., Opdyke, B., Roberts, A.P., 2021. Sea level and deep-sea temperature reconstructions suggest quasi-stable states and critical transitions over the past 40 million years. Sci. Adv. 7 (26), eabf5326.
Roser, B.P., Korsch, R.J., 1988. Provenance signatures of sandstone-mudstone suites determined using discriminant function analysis of major-element data. Chem. Geol. 67 (1–2), 119–139. https://doi.org/10.1016/0009-2541(88)90010-1.
Rousseau, R.M., 2001. Detection limit and estimate of uncertainty of analytical XRF results. Rig J 18 (2), 33–47.
Roy, P.D., Smykatz-Kloss, W., Sinha, R., 2006. Late Holocene geochemical history inferred from Sambhar and Didwana playa sediments, Thar Desert, India: comparison and synthesis. Quat. Int. 144 (1), 84–98. https://doi.org/10.1016/j.quaint.2005.05.018.
Roy, Priyadarsi D., Caballero, M., Lozano, R., Pi, T., Morton, O., 2009. Late pleistocene-holocene geochemical history inferred from lake tecocomulco sediments, basin of Mexico, Mexico. Geochem. J. 43 (1), 49–64. https://doi.org/10.2343/geochemj.1.0006.
Roy, P.D., Caballero, M., Lozano, R., Ortega, B., Lozano, S., Pi, T., Israde, I., Morton, O., 2010. Geochemical record of late quaternary paleoclimate from lacustrine sediments of paleo-lake san felipe, western sonora desert, Mexico. J. S. Am. Earth Sci. 29 (3), 586–596. https://doi.org/10.1016/j.jsames.2009.11.009.
Rubinić, V., Durn, G., Husnjak, S., Tadej, N., 2014. Composition, properties and formation of Pseudogley on loess along a precipitation gradient in the Pannonian region of Croatia. Catena 113, 138–149. https://doi.org/10.1016/j.catena.2013.10.003.
Rudra, K., 2018. In: Rudra, K. (Ed.), Evolution of the Bengal Basin BT - Rivers of the Ganga-Brahmaputra-Meghna Delta: A Fluvial Account of Bengal. Springer International Publishing. https://doi.org/10.1007/978-3-319-76544-0_2, 15–25.
Rühland, K., Phadtare, N.R., Pant, R.K., Sangode, S.J., Smol, J.P., 2006. Accelerated melting of Himalayan snow and ice triggers pronounced changes in a valley peatland from northern India. *Geophysical Research Letters, 33*(15). https://doi.org/10.1029/2006GL026704.
Saha, A., Roy, D.K., Khan, R., Ornee, T.I., Goswami, S., Idris, A.M., Biswas, P.K., Tamim, U., 2023. Provenance, weathering, climate and tectonic setting of Padma River sediments, Bangladesh: a geochemical approach. Catena 233, 107485. https://doi.org/10.1016/j.catena.2023.107485.
Sánchez-Bandera, C., Fagoaga, A., Serrano-Ramos, A., Solano-García, J., Barsky, D., DeMiguel, D., Ochando, J., Saarinen, J., Piñero, P., Lozano-Fernández, I., 2023. Glacial/interglacial climate variability in southern Spain during the late Early Pleistocene and climate backdrop for early Homo in Europe. Palaeogeogr. Palaeoclimatol. Palaeoecol. 625, 111688 https://doi.org/10.1016/j.palaeo.2023.111688.
Sawyer, E.W., 1986. The influence of source rock type, chemical weathering and sorting on the geochemistry of clasticsediments from the Quetico Metasedimentary Belt, Superior Province, Canada. Chem. Geol. 55, 77–95. https://doi.org/10.1016/0009-2541(86)90129-4.
Schatz, A.-K., Scholten, T., Kühn, P., 2015. Paleoclimate and weathering of the Tokaj (Hungary) loess–paleosol sequence. Palaeogeogr. Palaeoclimatol. Palaeoecol. 426, 170–182. https://doi.org/10.1016/j.palaeo.2015.03.016.
Shaman, J., Tziperman, E., 2005. The effect of ENSO on Tibetan Plateau snow depth: a stationary wave teleconnection mechanism and implications for the South Asian monsoons. J. Clim. 18 (12), 2067–2079.
Sheldon, N.D., 2003. Pedogenesis and geochemical alteration of the picture gorge subgroup, columbia river basalt. Oregon. Geological Society of America Bulletin 115 (11), 1377–1387. https://doi.org/10.1130/B25223.1.
Sheldon, N.D., 2006a. Abrupt chemical weathering increase across the Permian–Triassic boundary. Palaeogeogr. Palaeoclimatol. Palaeoecol. 231 (3–4), 315–321. https://doi.org/10.1016/j.palaeo.2005.09.001.
Sheldon, N.D., 2006b. Precambrian paleosols and atmospheric CO2 levels. Precambrian Res. 147 (1–2), 148–155.
Sheldon, N.D., 2006c. Quaternary glacial-interglacial climate cycles in Hawaii. J. Geol. 114 (3), 367–376.
Sheldon, N.D., Retallack, G.J., 2004. Regional paleoprecipitation records from the late eocene and oligocene of north America. J. Geol. 112 (4), 487–494.
Sheldon, N.D., Tabor, N.J., 2009. Quantitative paleoenvironmental and paleoclimatic reconstruction using paleosols. Earth Sci. Rev. 95 (1–2), 1–52. https://doi.org/10.1016/j.earscirev.2009.03.004.
Sheldon, N.D., Retallack, G.J., Tanaka, S., 2002. Geochemical climofunctions from North American soils and application to paleosols across the Eocene-Oligocene boundary in Oregon. J. Geol. 110 (6), 687–696.
Srivastava, A.K., Bansod, M.N., Singh, A., Sharma, N., 2019. Geochemistry of paleosols and calcretes from Quaternary sediments of Purna alluvial basin, central India: an emphasis on paleoclimate. Rhizosphere 11, 100162. https://doi.org/10.1016/j.rhisph.2019.100162.
Stiles, C.A., Stensvold, K.A., 2008. Loess contribution to soils forming on dolostone in the Driftless Area of Wisconsin. Soil Sci. Soc. Am. J. 72 (3), 650–659. https://doi.org/10.2136/sssaj2007.0112.
Stinchcomb, G.E., Nordt, L.C., Driese, S.G., Lukens, W.E., Williamson, F.C., Tubbs, J.D., 2016. A data-driven spline model designed to predict paleoclimate using paleosol geochemistry. Am. J. Sci. 316 (8), 746–777.
Tabor, Neil J., Myers, T.S., 2015. Paleosols as indicators of paleoenvironment and paleoclimate. Annu. Rev. Earth Planet Sci. 43, 333–361. https://doi.org/10.1146/annurev-earth-060614-105355.
Tabor, N.J., Myers, T.S., Michel, L.A., 2017. Sedimentologist's guide for recognition, description, and classification of paleosols. Terrestrial Depositional Systems. Elsevier, pp. 165–208. https://doi.org/10.1016/B978-0-12-803243-5.00004-2.
Varela, A.N., Raigemborn, M.S., Santamarina, P.E., Lizzoli, S., Adatte, T., Heimhofer, U., 2021. Carbon isotopic signature and organic matter composition of cenomanian high-latitude paleosols of Southern Patagonia. Geosciences, 11(9) 378. https://doi.org/10.3390/geosciences11090378.
Wang, Y., Cheng, H., Edwards, R.L., He, Y., Kong, X., An, Z., Wu, J., Kelly, M.J., Dykoski, C.A., Li, X., 2005. The Holocene Asian monsoon: links to solar changes and North Atlantic climate. Science 308 (5723), 854–857. https://doi.org/10.1126/science.1106296.
Wang, Y., Cheng, H., Edwards, R.L., Kong, X., Shao, X., Chen, S., Wu, J., Jiang, X., Wang, X., An, Z., 2008. Millennial-and orbital-scale changes in the East Asian monsoon over the past 224,000 years. Nature 451 (7182), 1090–1093. https://doi.org/10.1038/nature06692.
Wang, W., Gan, Z., Zhang, X., Li, S., Xu, Y., 2022. Temporal variation in the chemical index of alteration in Early Cretaceous black shale as a proxy for paleoclimate. J. Geol. 130 (5), 393–411.
Wang, T.-H., Wang, Q.-B., Han, C.-L., Cui, D., Sauer, D., 2023. Development and application of new transfer functions between climate and soil weathering indices for paleoclimatic reconstructions from Chinese loess-paleosol sections. Catena 224, 106974. https://doi.org/10.1016/j.catena.2023.106974.
Warrick, R.A., Ahmed, Q.K., 1996. The Implications of Climate and Sea-Level Change for Bangladesh. Kluwer Academic Publications, The Netherlands.
Wright, V.P., 1992. Paleopedology: stratigraphic relationships and empirical models. Dev. Earth Surf. Process 2, 475–499. https://doi.org/10.1016/B978-0-444-89198-3.50023-4. Elsevier.
Yadav, R.R., Singh, J., 2002. Tree-ring-based spring temperature patterns over the past four centuries in western Himalaya. Quaternary Research 57 (3), 299–305. https://doi.org/10.1006/qres.2002.2337.
Yan, D., Chen, D., Wang, Q., Wang, J., 2010. Large-scale climatic fluctuations in the latest Ordovician on the Yangtze block, south China. Geology 38 (7), 599–602. https://doi.org/10.1130/G30961.1.
Yang, S., Liu, L., Chen, H., Tang, G., Luo, Y., Liu, N., Li, D., 2021. Variability and environmental significance of organic carbon isotopes in Ganzi loess since the last interglacial on the eastern Tibetan Plateau. Catena 196, 104866. https://doi.org/10.1016/j.catena.2020.104866.
Zhang, J., Crowley, T.J., 1989. Historical climate records in China and reconstruction of past climates. J. Clim. 833–849.
Zimmermann, B., Schleser, G.H., Bräuning, A., 1997. Preliminary results of a Tibetan stable C-isotope chronology dating from 1200 to 1994. Isot. Environ. Health Stud. 33 (1–2), 157–165. https://doi.org/10.1080/10256019808036367.